




SNP rs4971059 predisposes to breast carcinogenesis and chemoresistance via TRIM46-mediated HDAC1 degradation

Zihan Zhang¹, Xiaoping Liu^{1,2}, Lei Li³, Yang Yang⁴, Jianguo Yang^{1,2}, Yue Wang^{2,5}, Jiajing Wu⁵, Xiaodi Wu⁵, Lin Shan⁵, Fei Pei⁶, Jianying Liu⁶, Shu Wang⁴, Wei Li⁷, Luyang Sun¹ , Jing Liang^{1,*}  & Yongfeng Shang^{1,2,5,*} 

Abstract

Identification of the driving force behind malignant transformation holds the promise to combat the relapse and therapeutic resistance of cancer. We report here that the single nucleotide polymorphism (SNP) rs4971059, one of 65 new breast cancer risk loci identified in a recent genome-wide association study (GWAS), functions as an active enhancer of *TRIM46* expression. Recreating the G-to-A polymorphic switch caused by the SNP via CRISPR/Cas9-mediated homologous recombination leads to an overt upregulation of *TRIM46*. We find that *TRIM46* is a ubiquitin ligase that targets histone deacetylase HDAC1 for ubiquitination and degradation and that the *TRIM46*-HDAC1 axis regulates a panel of genes, including ones critically involved in DNA replication and repair. Consequently, *TRIM46* promotes breast cancer cell proliferation and chemoresistance *in vitro* and accelerates tumor growth *in vivo*. Moreover, *TRIM46* is frequently overexpressed in breast carcinomas, and its expression is correlated with lower HDAC1 expression, higher histological grades, and worse prognosis of the patients. Together, our study links SNP rs4971059 to replication and to breast carcinogenesis and chemoresistance and support the pursuit of *TRIM46* as a potential target for breast cancer intervention.

Keywords breast cancer; HDAC1; replication; SNP; *TRIM46*

Subject Categories Cancer; Chromatin, Transcription & Genomics;

Post-translational Modifications & Proteolysis

DOI 10.15252/emboj.2021107974 | Received 9 February 2021 | Revised 28 June

2021 | Accepted 16 August 2021 | Published online 30 August 2021

The EMBO Journal (2021) 40: e107974

Introduction

Genetic aberrance is the key element in fostering the adaptation and evolution of cancer cells, and identification of the driving node behind genome aberrations holds the promise to decipher malignant transformation and ultimately to combat therapeutic resistance and relapse of cancer. Despite the extensive effort in cancer genomics, identification of driver genes remains a daunting task, and differentiation of drivers from passengers in oncogenesis remains a major bottleneck in understanding the essence of cancer development and progression (Vogelstein *et al*, 2013). In recent years, genome-wide association study (GWAS) has become a powerful approach to identify the genetic contribution to the risk of cancer. Unlike traditional candidate-driven studies, GWAS studies compare the entire genomic sequence from a large population of cancer patients to the healthy population, making the search for genetic aberrance in cancer more objective. Ultimately, potential drivers identified by different sources and via various means need mechanistic exploration and experimental validation.

In a recent GWAS analysis of breast cancer in 122,977 cases and 105,974 control patients of European ancestry and 14,068 cases and 13,104 control patients of East Asian ancestry, 65 new loci were identified to be associated with overall breast cancer risk at $P < 5 \times 10^{-8}$ (Michailidou *et al*, 2017). Interestingly, most of the credible-risk single nucleotide polymorphisms (SNPs) in these loci map to distal gene-regulatory elements. One of these risk loci is SNP rs4971059. However, whether and how this locus might be functionally linked to breast carcinogenesis need to be investigated.

The tripartite motif (TRIM) protein family is composed of more than 70 members, characterized by the presence of an N-terminal RING-finger domain (R), one or two B-box domains (B), and a

1 Department of Biochemistry and Biophysics, School of Basic Medical Sciences, Key Laboratory of Carcinogenesis and Translational Research (Ministry of Education), Peking University Health Science Center, Beijing, China

2 Department of Biochemistry and Molecular Biology, School of Basic Medical Sciences, Hangzhou Normal University, Hangzhou, China

3 Institute of Systems and Physical Biology, Shenzhen Bay Laboratory, Shenzhen, China

4 Breast Disease Center, Peking University People's Hospital, Beijing, China

5 Department of Biochemistry and Molecular Biology, School of Basic Medical Sciences, Capital Medical University, Beijing, China

6 Department of Pathology, School of Basic Medical Sciences, Peking University Health Science Center, Beijing, China

7 Department of Biological Chemistry, University of California Irvine, Irvine, CA, USA

*Corresponding author. Tel: +86 10 82805118; Fax: +86 10 82801355; E-mail: liang_jing@hsc.pku.edu.cn

**Corresponding author. Tel: +86 10 82805118; Fax: +86 10 82801355; E-mail: yshang@hsc.pku.edu.cn

coiled-coil domain (C) (Short & Cox, 2006; Chu & Yang, 2011; Herquel *et al*, 2011). It has been reported that several members of the TRIM family, including TRIM24, TRIM27, TRIM33, and TRIM66, possess E3 ubiquitin ligase activity attributable to the RING domain (Jain *et al*, 2014; Chen *et al*, 2015; Xue *et al*, 2015; Wang *et al*, 2016). Functionally, TRIM proteins have been implicated in a broad range of biological processes including transcription regulation, cell growth, apoptosis, development, and tumorigenesis (Hatakeyama, 2011, 2017; Harterink *et al*, 2019; Venuto & Merla, 2019). However, the molecular function of TRIM46 remains to be explored, and whether and how this TRIM protein is involved in breast carcinogenesis is currently unknown.

Histone deacetylase 1 (HDAC1) represents a paradigm of a group of epigenetic enzymes catalyzing the removal of acetyl moieties from histone lysine residues, leading to chromatin compaction and transcription silencing (Gregoretto *et al*, 2004; Brunmeir *et al*, 2009). In effect, HDAC1 is often associated with HDAC2 as a heterodimer and engaged in several prominent corepressor assemblies including the NuRD, Sin3A, and CtBP complexes (Hassig *et al*, 1997; Zhang *et al*, 1999; You *et al*, 2001). It is reported that HDAC1 is overexpressed in various types of cancer (Choi *et al*, 2001; Eom *et al*, 2012). Accordingly, HDAC inhibitors have been pursued as promising therapeutics for cancer treatment regimen (Li & Seto, 2016). However, evidence also indicates that HDAC1 is downregulated (Suzuki *et al*, 2009) and acting as a tumor suppressor under certain circumstances (Santoro *et al*, 2013), suggesting a context-dependent scheme of actions for HDAC1 in cancer development. Importantly, as most of its gene expression profiling has been conducted at the mRNA level, whether and how HDAC1 is regulated at the protein level under pathophysiological conditions need further delineation.

In this study, we report that the recently identified breast cancer risk locus SNP rs4971059 resides in the sixth intron and within an active enhancer element of the *TRIM46* gene. We find that a G to A polymorphic switch of the rs4971059 allele boosts the activity of this enhancer and leads to an overt upregulation of *TRIM46* expression. We demonstrate that *TRIM46* acts as an E3 ligase that targets HDAC1 for ubiquitination and degradation. We show that the *TRIM46*-HDAC1 axis functionally intersects with DNA replication and repair pathways to promote carcinogenesis and chemoresistance in breast cancer. We explore the clinicopathological significance of the *TRIM46*-HDAC1 axis in breast cancer.

Results

SNP rs4971059 locates at the sixth intron of *TRIM46* gene that functions as an active enhancer

As mentioned above, a recent GWAS study of breast cancer identified 65 new breast cancer risk loci (Michailidou *et al*, 2017). One of the loci, SNP rs4971059, is mapped to chromosome 1q22. Bioinformatics analysis indicates that this locus is at the sixth intron of *TRIM46* gene (Fig 1A). HaploReg scanning (Ward & Kellis, 2012) reveals that the region surrounding SNP rs4971059 is marked with histone H3 lysine 4 mono-methylation (H3K4me1) (Fig 1B, left), an eminent feature of an active enhancer (Calo & Wysocka, 2013). Indeed, chromatin immunoprecipitation (ChIP) assays in breast adenocarcinoma MCF-7 cells confirmed a significant enrichment of

H3K4me1 as well as H3K27 acetylation (H3K27ac) on a fragment spanning ± 300 bp of the SNP, whereas the typical promoter mark H3K4 tri-methylation (H3K4me3) was barely detected (Fig 1B, right). To further support the enhancer nature of the sequence surrounding SNP rs4971059, we chemically synthesized a 1.1-kb DNA fragment containing this SNP. We cloned it into a luciferase reporter driven by a minimal SV40 promoter (Ochs *et al*, 2012). Wild-type SNP[G] was generated first, and the risk SNP[A] was subsequently created by site-directed mutagenesis. Transfection of MCF-7 cells with control reporters or reporter constructs containing SNP[G] or SNP[A] fragments and measurement of the luciferase activity showed that compared to control reporters, the reporter construct containing wild-type SNP[G] exhibited an elevated transcriptional activity (Fig 1C). Remarkably, the reporter activity was further boosted in cells transfected with SNP[A] rs4971059-containing fragments (Fig 1C). We additionally cloned a 3.25-kb fragment of *TRIM46* promoter and constructed a PGL3-*TRIM46* luciferase reporter. The 1.1-kb fragments containing SNP[G] or SNP[A] were then cloned to this reporter. Similar experiments were performed in MCF-7 cells, and the results were consistent with that for SV40 promoter (Fig 1C). These observations suggest a gain-of-function change of the enhancer element driven by a G to A switch of SNP rs4971059. We further performed chromosome conformation capture (3C) assays to examine its interaction with the *TRIM46* promoter (Ling *et al*, 2006). PCR primers were designed near the end of DpnII fragments in the same orientation to successive restriction fragments (Appendix Table S2). SNP rs4971059 resides in 3C fragment 17. When a constant primer and a probe in fragment 17 were used in the 3C assay, we observed a strong interaction with fragment 5, the genomic region 3-kb upstream of the transcription start site of *TRIM46*. When a constant primer and a probe in fragment 5 were used in the 3C assay, we observed strong physical interactions with fragment 17. The results clearly showed a loop structure formation between the SNP rs4971059-containing region with the *TRIM46* promoter (Fig 1D), supporting the notion that the sequence surrounding SNP rs4971059 is implemented to regulate *TRIM46* expression *in vivo*.

To further support the notion that the SNP rs4971059-containing region is an enhancer element for the regulation of *TRIM46* expression and to extend our observations to a pathophysiologically relevant context, we collected 90 tumor samples from breast cancer patients, whose clinical and pathologic characteristics are known (Table EV1). Genomic DNAs and total RNAs were extracted from tissue homogenates. DNA fragments surrounding the rs4971059 locus were then subjected to Sanger sequencing, and total RNAs were subjected to real-time reverse transcriptase (RT)-PCR (qPCR) analysis. Remarkably, eQTL analysis revealed that the risk allele rs4971059 was strongly correlated with an increased expression of *TRIM46* (false discovery rate [FDR] = 0.00147; Fig 1E).

To strengthen the functional link between the risk locus SNP rs4971059 and the expression of *TRIM46*, we next examined the genotypes of several commonly used breast cancer cell lines, including MCF-7, T47D, and MDA-MB-231, and a non-tumorigenic human breast epithelial cell line MCF-10A. Sanger sequencing of the PCR amplicons revealed heterozygous rs4971059 in cancer cells, with a variable peak height ratio of G to A (Fig EV1A). We then performed TA cloning for MCF-7 cells in an attempt to quantify the ratio of different alleles. Out of 20 TA clones sequenced, we found

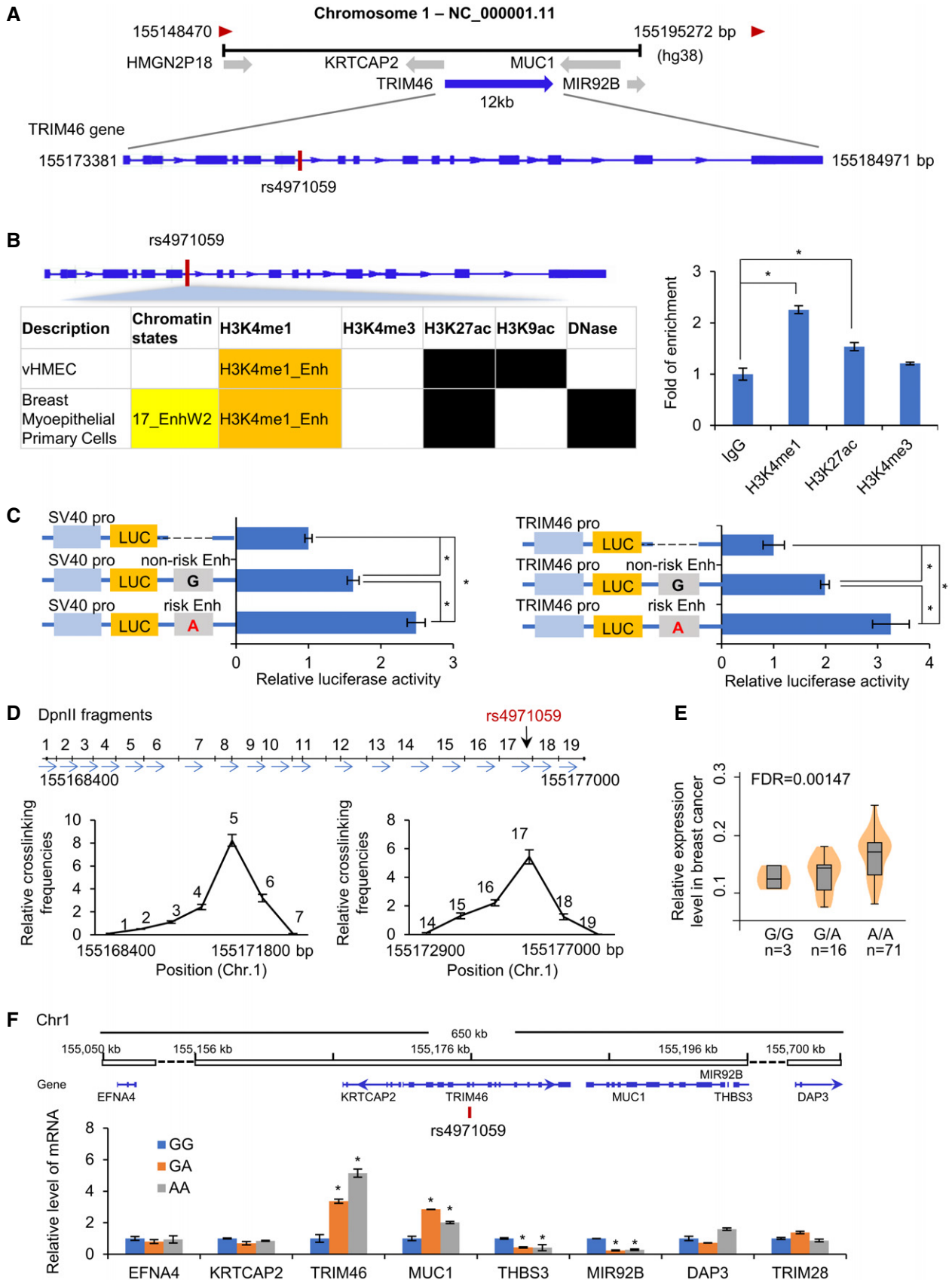


Figure 1.

Figure 1. SNP rs4971059 locates in an active enhancer at the 6th intron of TRIM46.

- A Physical map of the locus of *TRIM46* [chromosome 1: 155173381–155184971 (hg38)] and SNP rs4971059 [chromosome 1: 155176305 (hg38)].
- B HaploReg v4.1 was used to predict the potential functions of SNP rs4971059 (left). The yellow box means “Weak Enhancer 2” (H3K4me1 and DNase enrichment), the orange box means “H3K4me1 Enhancer”, and the black box means “missing data”. ChIP assays were performed with antibodies against H3K4me1, H3K4me3, or H3K27Ac in the region surrounding SNP rs4971059 (right).
- C Luciferase assays showing enhancer activity in the SNP rs4971059 region in MCF-7 cells. MCF-7 cells were transfected with the indicated promoters: PGL3-SV40, PGL3-SV40-SNP[G] or PGL3-SV40-SNP[A] (left); PGL3-TRIM46, PGL3-TRIM46-SNP[G]; or PGL3-TRIM46-SNP[A] (right). Forty-eight hours after the transfection, luciferase activity was measured. Relative luciferase activity was calculated as firefly luciferase activity divided by renilla luciferase activity and shown relative to the control.
- D The SNP rs4971059-containing region formed close contact with the promoter of *TRIM46* in a 3C assay. DpnII fragments in 1q22 were shown on the top panel (hg38). SNP rs4971059 resides in 3C fragment 17, and fragment 5 is in the genomic region 3-kb upstream of the TSS of *TRIM46*. PCR primers were designed near the end of DpnII fragments in the same orientation, and 3C assays were performed with a constant primer in fragment 17 (lower-left panel) or a constant primer in fragment 5 (lower-right panel).
- E eQTL analysis demonstrating the correlation between rs4971059 genotype and expression of *TRIM46*. The panel showed results from breast cancer tissues obtained from the mastectomy of the patients. In the boxplot, the central lines, the box limits, and the whiskers represented medians, 25th/75th percentile, and min/max, respectively (FDR = 0.00147).
- F A physical 650-kb window of the genomic distribution of genes surrounding SNP rs4971059, such as *EFNA4*, *KRTCAP2*, *MUC1*, *MIR92B*, *THBS3*, and *DAP3* (top). Total RNAs were extracted from [GG], [GA], or [AA] MCF-10A cells and analyzed for the expression of *EFNA4*, *KRTCAP2*, *TRIM46*, *MUC1*, *THBS3*, *MIR92B*, or *DAP3* by RT-qPCR. *TRIM28* was examined as a negative control (bottom).
- Data information: In (B, C, D, and F), each bar represents the mean \pm SD for biological triplicate experiments (* $P < 0.05$, two-tailed unpaired t-test).

13/7 of G/A ratio in the risk locus (Fig EV1B), suggesting mixed genotypes within the cell population (Fig EV1C), possibly due to spontaneous mutation after multiple passage numbers *in vitro*.

Interestingly, compared to the tested cancer cells, MCF-10A cells exhibited a highly homogeneous [GG] genotype of SNP rs4971059 (Fig EV1A). We then isolated single cell-derived [GG] MCF-10A cells and performed gene editing using CRISPR/Cas9-mediated homologous recombination to obtain [GA] and [AA] cells (Fig EV1D). Real-time qPCR showed significantly elevated mRNA levels of *TRIM46* upon G to A change in SNP rs4971059 (Fig 1F), supporting that the risk allele SNP rs4971059A is linked to upregulation of *TRIM46*. Meanwhile, we also examined the expression of *KRTCAP2*, *THBS3*, *MIR92B*, *MUC1*, *EFNA4*, and *DAP3* in different genotypic MCF-10A cells. These genes were chosen because they were proximal to SNP rs4971059 in the linear distance (< 20 kb) or significantly associated with the locus according to eQTL analysis (Michailidou *et al*, 2017). The expression of remotely located *TRIM* family protein *TRIM28* was examined as a negative control. Among all genes analyzed, qPCR showed the strongest and proportional association between the number of A alleles and the mRNA levels of *TRIM46* (Fig 1F). Together, these observations indicate that the SNP rs4971059-containing region in the 6th intron of *TRIM46* gene is an enhancer element for the gene and that the G to A polymorphic switch is a gain-of-function mutation that is associated with an increased expression of *TRIM46* in breast cancer.

TRIM46 is physically associated with HDAC1 in breast cancer cells

Given the GWAS identification of SNP rs4971059 as one of the risk loci for breast carcinogenesis (Michailidou *et al*, 2017) and our observations of the physical and functional association of this locus with *TRIM46*, to understand the molecular basis underlying the role of SNP rs4971059 in breast cancer susceptibility, we next investigated the biological activity of *TRIM46* in breast cancer cells. To this end, affinity purification coupled with mass spectrometry was utilized first to interrogate the *TRIM46* interactome *in vivo*. In these experiments, whole-cell extracts were prepared from MCF-7 cells stably expressing FLAG-tagged *TRIM46* (FLAG-*TRIM46*) and

subjected to affinity purification using an anti-FLAG affinity column. The purified protein complexes were resolved on SDS-PAGE and silver-stained, and the protein bands were retrieved and analyzed by mass spectrometry. The results showed that *TRIM46* was co-purified with a list of proteins, including HDAC1, JMJD3, and WDR5 (Fig 2A). The detailed results of the mass spectrometric analysis are provided in Table EV2.

As mentioned earlier, *TRIM* family proteins contain a RING domain, and several members of this family have been characterized as E3 ligases (Jain *et al*, 2014; Xue *et al*, 2015). Thus, it is plausible to postulate that *TRIM46* is also functionally linked to protein stability. To test this, we next transfected MCF-7 cells with a control vector or *TRIM46* expression plasmid in the presence or absence of MG132. Western blotting analysis showed that overexpression of *TRIM46* had no effect on the protein levels of SIN3B, RBBP4/7, WDR5, HDAC2, PARP1, LSD1, and HAT1, and even caused an increase in the level of JMJD3, possibly due to an indirect mechanism (Fig 2B). However, overexpression of *TRIM46* resulted in a significant and reproducible decrease in HDAC1 protein level, which was almost abrogated in the presence of MG132 (Fig 2B), suggesting that *TRIM46* negatively affects the stability of HDAC1, a function that is in line with its potential E3 ligase activity as a member of *TRIM* family. Interestingly, the protein level of HDAC2 was increased in *TRIM46*-overexpressed MCF-7 cells, which was abrogated in the presence of MG132. The upregulation of HDAC2 is likely due to a compensatory effect of HDAC1 loss, as Western blotting revealed increased expression of HDAC2 upon knockdown of HDAC1 (Fig EV2A), consistent with the previous study performed in other biological contexts (Lagger *et al*, 2010; Chen *et al*, 2011).

To verify the physical interaction of *TRIM46* with HDAC1 in breast cancer cells, we prepared cellular extracts from MCF-7 cells. Co-immunoprecipitation (Co-IP) assays with antibodies against *TRIM46* followed by immunoblotting with an antibody against HDAC1 confirmed the interaction between *TRIM46* and HDAC1 (Fig 2C). In addition, GST pull-down experiments with bacterially expressed GST-*TRIM46* and *in vitro* transcribed/translated HDAC1 further validated the interaction of *TRIM46* with HDAC1 (Fig 2D). Moreover, GST pull-down experiments with GST-fused *TRIM46* deletion mutants and *in vitro* transcribed/translated HDAC1

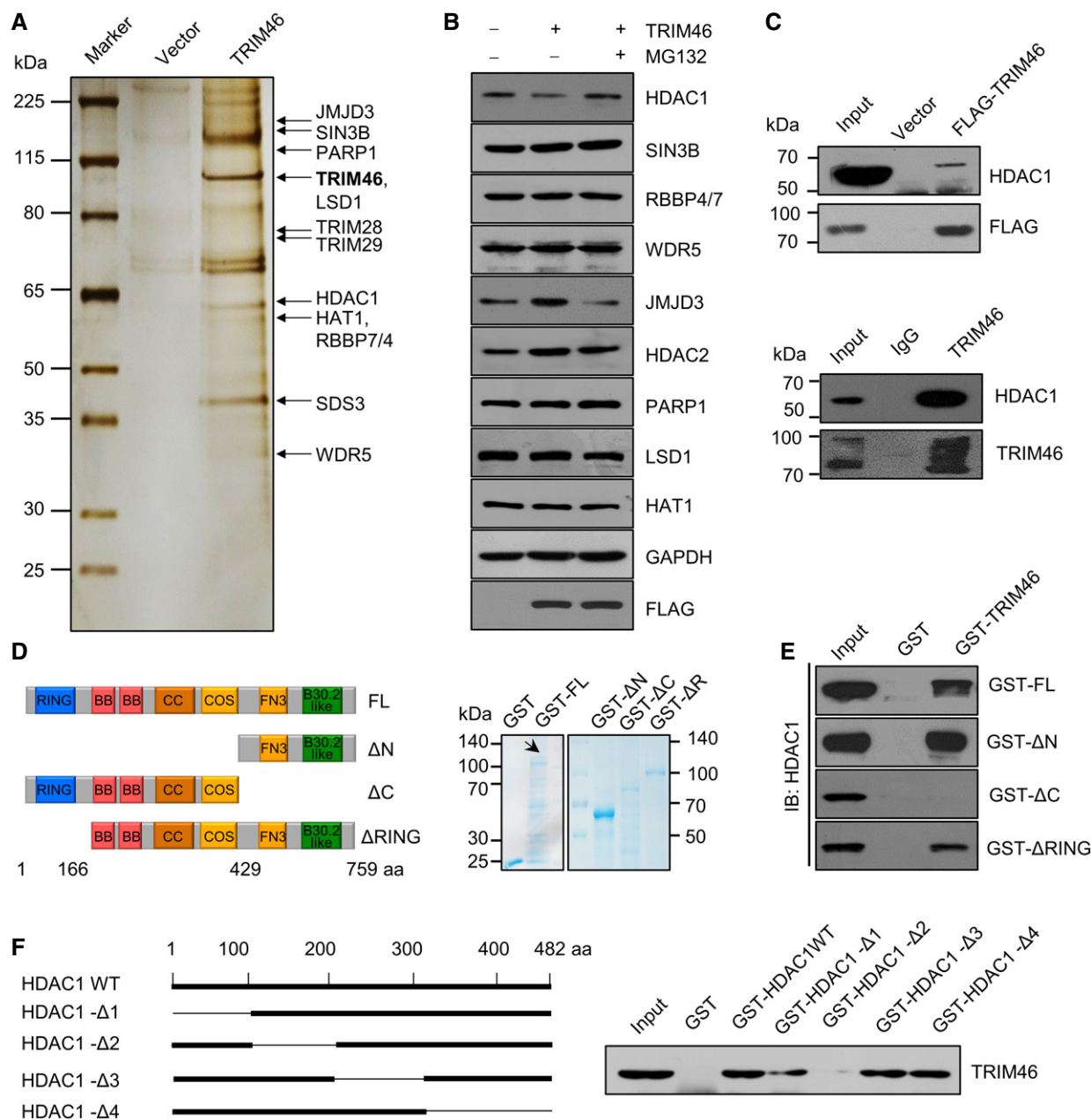


Figure 2. TRIM46 is physically associated with HDAC1.

- A** Mass spectrometry analysis of TRIM46-associated proteins. Whole-cell extracts from MCF-7 cells stably expressing FLAG-TRIM46 were subjected to affinity purification with anti-FLAG immobilized on the agarose beads. The purified protein complex was resolved on SDS-PAGE and silver-stained. The bands were retrieved and analyzed by mass spectrometry.
- B** MCF-7 cells were transfected with a control vector or FLAG-TRIM46 for 40 h and treated with DMSO or MG132 (2 μ M) for 10 h. Cellular lysates were then collected for Western blotting with antibodies against the indicated proteins.
- C** MCF-7 cells were transfected with control vector or FLAG-TRIM46 for 48 h. Whole-cell lysates were prepared, and immunoprecipitation was performed with anti-FLAG followed by immunoblotting with antibodies against indicated proteins (top). Immunoprecipitation assays in MCF-7 cells with anti-TRIM46 followed by immunoblotting with antibodies against the indicated proteins (bottom).
- D** Schematic diagrams of TRIM46 deletion mutants (left). Coomassie brilliant blue (CBB) staining of GST-fused proteins as indicated (right). GST-FL was shown with the arrow.
- E** GST pull-down experiments were performed with bacterially expressed GST-fused proteins as shown and *in vitro* transcribed/translated full-length HDAC1.
- F** Schematic diagrams of HDAC1 deletion mutants. GST pull-down experiments were performed with bacterially expressed GST-fused proteins as indicated and *in vitro* transcribed/translated TRIM46.

Source data are available online for this figure.

revealed that the C-terminal of TRIM46 containing the FN3 and B30.2 domains is responsible for the interaction of TRIM46 with HDAC1 (Fig 2E), consistent with the receptor-substrate interaction typically seen for E3 ligases (Hatakeyama, 2017). Reciprocally, GST pull-down experiments with GST-fused HDAC1 deletion mutants and *in vitro* transcribed/translated TRIM46 showed that the region containing 101–200 aa of HDAC1 is responsible for the interaction with TRIM46 (Fig 2F).

TRIM46 is an E3 ubiquitin ligase that targets HDAC1 for ubiquitination and degradation

Given that several members of the TRIM family proteins have been characterized as E3 ligases (Jain *et al*, 2014; Xue *et al*, 2015), as stated above, to explore the biological significance of the physical interaction between TRIM46 and HDAC1, we next investigated whether TRIM46 also acts as an E3 ligase and targets HDAC1 for ubiquitination and degradation. To this end, experiments with gain-of-function and loss-of-function of TRIM46 were performed in MCF-7 cells, and the protein level of HDAC1 was measured. Western blotting of cellular lysates revealed that overexpression of TRIM46 was associated with a decrease, in a dose-dependent manner, in HDAC1 protein but not its mRNA level, an effect that was abolished upon treatment of the cells with MG132 (Fig 3A). We also isolated cells containing [GG], [GA], or [AA] in SNP rs4971059 from single cell-derived MCF-7 clones. Western blotting revealed upregulated TRIM46 protein and downregulated HDAC1 protein in [AA] cells compared to [GG] or [GA] cells, supporting that SNP rs4971059A is correlated with increased TRIM46 expression and decreased HDAC1 (Fig 3B). Higher TRIM46 expression and lower HDAC1 protein levels were also observed in previously generated [AA] MCF-10A cells compared to cells with the other two genotypes (Fig 3C and D), supporting that overexpression of TRIM46 lead to a decrease of HDAC1 protein. On the other hand, knockdown of TRIM46 expression in MCF-7 cells led to an increase in HDAC1 protein level, an effect that was effectively rescued by overexpression of a siRNA-resistant TRIM46 construct (Fig 3E). Moreover, cycloheximide (CHX) chase assays showed that TRIM46 overexpression was

associated with an evident decrease in the half-life of HDAC1, but only in the absence of MG132 (Fig 3F and G). Consistently, knockdown of TRIM46 increased the half-life of HDAC1 (Fig 3H). These observations suggest that TRIM46 targets HDAC1 for degradation through the proteasome-mediated process.

A key event in proteasome-mediated protein degradation is the ubiquitination of the target protein (Micel *et al*, 2013). To support the notion that TRIM46 targets HDAC1 for degradation, we next investigated whether TRIM46 affects HDAC1 ubiquitination. To this end, *in vitro* ubiquitination assays were performed first. Incubation of bacterially expressed GST-HDAC1 with eukaryotically purified FLAG-TRIM46, plus commercial ubiquitin-activating enzyme (E1), ubiquitin-conjugating enzymes (E2), and ubiquitin, and analysis by Western blotting detected polyubiquitinated HDAC1 species, but only when both E2 and ubiquitin were added and wild-type TRIM46 was used; incubation of GST-HDAC1 with FLAG-TRIM46 Δ RING or FLAG-TRIM46 Δ C resulted in no detectable HDAC1 polyubiquitination (Fig 4A). Consistently, *in vivo* ubiquitination assays in MCF-7 cells showed that depletion of TRIM46 resulted in a decreased HDAC1 polyubiquitination (Fig 4B), whereas overexpression of TRIM46 led to an increased HDAC1 polyubiquitination (Fig 4C). Further experiments with TRIM46 deletion mutants revealed that both the RING domain and the C-terminal region of TRIM46 are required for HDAC1 polyubiquitination (Fig 4D). Together, these data indicate that TRIM46 promotes HDAC1 polyubiquitination.

We then co-transfected MCF-7 cells with Myc-TRIM46 together with FLAG-HDAC1 or FLAG-tagged serial deletions of HDAC1 (HDAC1 Δ 1-HDAC1 Δ 4). Western blotting analysis of cellular lysates showed that overexpression of TRIM46 was associated with an increase in polyubiquitination and a decrease in the protein level of wild-type HDAC1 (Fig 4E and F). Similar results were also obtained for HDAC1 deletion mutants, except for HDAC1 Δ 2 (Fig 4E and F), suggesting that TRIM46-targeted polyubiquitination occurs in 100–200 aa of HDAC1. Among lysine (K) sites in the 100–200 aa of HDAC1, K123, K126, K143, and K144 are predicted as ubiquitination sites in HDAC1 by Protein Lysine Modifications Database (PLMD). Indeed, mutations of K123, K143, and K144 to arginine (R)

Figure 3. TRIM46 negatively regulates HDAC1.

- A TRIM46 negatively regulates the steady-state level of the HDAC1 protein. MCF-7 cells were transfected with increasing amounts of FLAG-TRIM46. 48 h after transfection, cells were treated with DMSO or MG132 for 10 h before cells were collected for Western blotting (left). Alternatively, total RNAs were extracted and analyzed for HDAC1 expression by RT-qPCR (right).
- B Cellular proteins were extracted from [GG], [GA], or [AA] MCF-7 cells, and Western blotting was performed with polyclonal antibodies against TRIM46, HDAC1, and GAPDH.
- C Cellular proteins were extracted from [GG], [GA], or [AA] MCF-10A cells, and Western blotting was performed with polyclonal antibodies against TRIM46, HDAC1, or GAPDH.
- D Total RNAs were extracted from [GG], [GA], or [AA] MCF-10A cells and analyzed for HDAC1 expression by RT-qPCR.
- E MCF-7 cells were transfected with control siRNA, TRIM46 siRNA, or a siRNA-resistant TRIM46 construct together with TRIM46 siRNA. Western blotting (left) and RT-qPCR (right) were performed as in A.
- F MCF-7 cells were transfected with empty vector or FLAG-TRIM46 for forty-eight hours and then treated with 50 μ g/ml cycloheximide (CHX) for the indicated hours. DMSO was added to cells 10 h before cellular proteins were collected for Western blotting (left). On the right panel, quantitation was done by densitometry analysis of the immunoblots and expressed as signals of HDAC1.
- G MCF-7 cells were treated as described in F, except that MG132 (10 μ M) was added to cells 10 h before cellular proteins were collected for Western blotting (left). Quantitation was performed on the right panel as in F.
- H MCF-7 cells were treated with control siRNA or TRIM46 siRNA. Forty-eight hours after transfection, cells were treated with 50 μ g/ml CHX for the indicated hours before cellular proteins were extracted for Western blotting analysis (left). Quantitation was performed on the right panel as in F.

Data information: In (A, D, E, F, G, and H), each bar represents the mean \pm SD for biological triplicate experiments (* P < 0.05, ** P < 0.01, two-tailed unpaired t -test). Source data are available online for this figure.

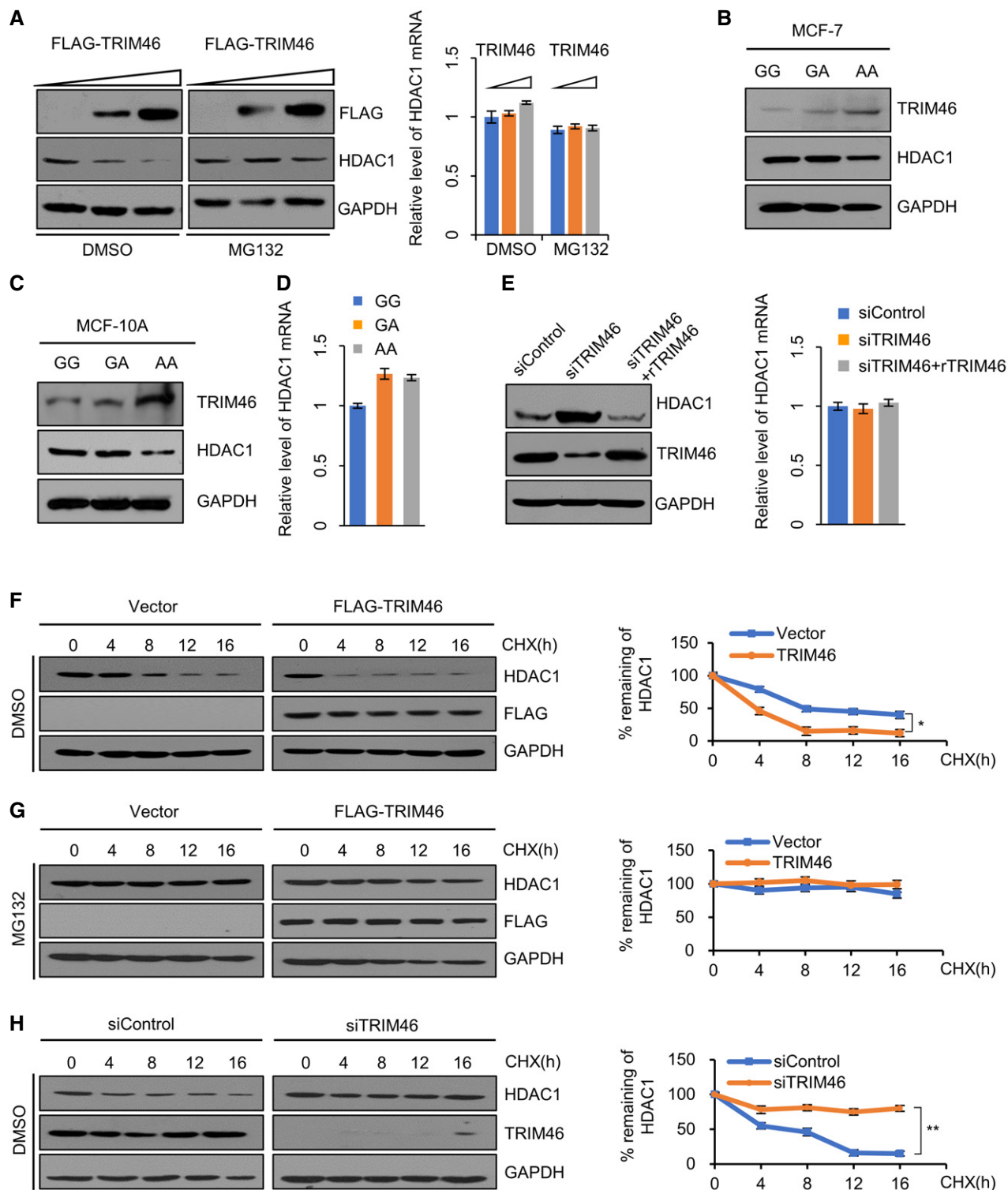


Figure 3.

abolished TRIM46-mediated polyubiquitination and degradation of HDAC1 (Fig 4G and H), suggesting these sites of HDAC1 are targeted by TRIM46. Together, these results indicate that TRIM46 targets HDAC1 for polyubiquitination and degradation and that TRIM46 is a *bona fide* E3 ubiquitin ligase for HDAC1.

The TRIM46-HDAC1 axis intersects with DNA replication and repair

As mentioned earlier, HDAC1 exists in multiple corepressor complexes that function in chromatin compaction and transcription

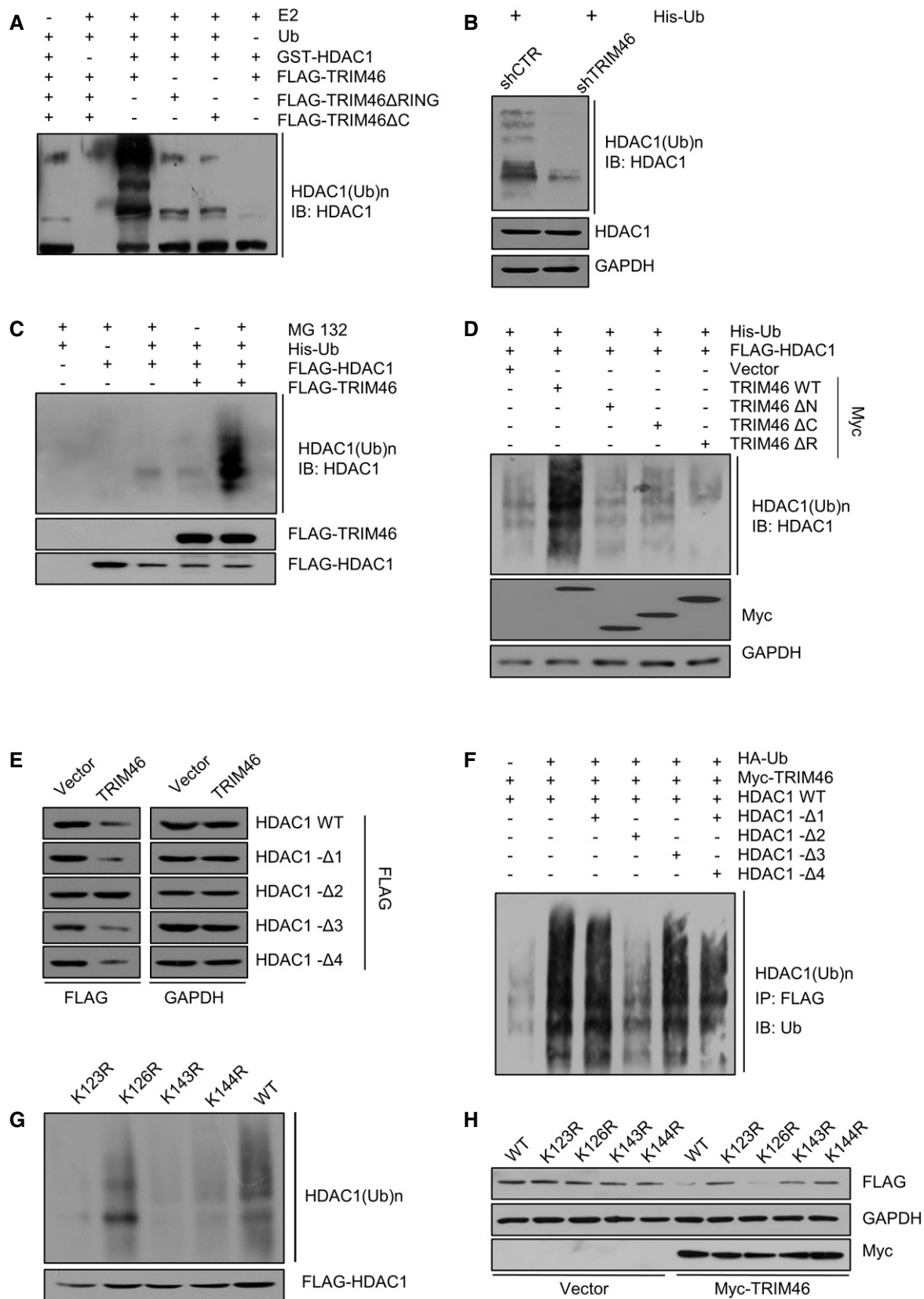


Figure 4.

Figure 4. TRIM46 promotes HDAC1 ubiquitination and degradation.

- A In vitro ubiquitination assays with GST-HDAC1, FLAG-TRIM46, FLAG-TRIM46 Δ RING, or FLAG-TRIM46 Δ C in the presence or absence of ubiquitin and E2. HDAC1 was detected using Western blotting.
- B–D In vivo ubiquitination assays performed in MCF-7 cells. (B) Stable shCTR- or shTRIM46-expressing MCF7 cells were transfected with His-Ub for 40 h. Cells were then treated with MG132 (10 μ M) for 12 h before Ni-NTA bead precipitation followed by IB with anti-HDAC1. (C and D) MCF-7 cells were co-transfected with the indicated plasmids. Forty-eight hours after transfection, cells were treated with MG132 for 10 h before cellular extracts were harvested for Ni-NTA bead precipitation followed by IB with anti-HDAC1.
- E MCF-7 cells were co-transfected with Myc-TRIM46 and FLAG-tagged wild-type HDAC1 or HDAC1 deletion mutants for 48 h. Cellular proteins were extracted for western blotting analysis.
- F MCF-7 cells were co-transfected with Myc-TRIM46, HA-ubiquitin, and FLAG-tagged wild-type HDAC1 or HDAC1 mutants for 40 h. Cells were treated with MG132 for 12 h before cellular extracts were prepared for immunoprecipitation assays with anti-FLAG followed by immunoblotting with anti-ubiquitin.
- G MCF-7 cells were co-transfected with FLAG-HDAC1-K123R, K126R, K143R, or K144R along with indicated plasmids for 40 h. Cells were treated with MG132 (10 μ M) for 10 h before cellular extracts were prepared for Ni-NTA bead precipitation.
- H MCF-7 cells were co-transfected with Myc-TRIM46 and wild-type HDAC1 or indicated HDAC1 mutants for 48 h. Cellular proteins were extracted for Western blotting analysis.

Source data are available online for this figure.

repression (Gregoret *et al*, 2004; Brunmeir *et al*, 2009). To understand the biological significance of TRIM46-mediated HDAC1 degradation, we first performed chromatin immunoprecipitation-coupled DNA sequencing (ChIP-seq) to investigate the effect of TRIM46 on chromatin targeting of HDAC1. In these experiments, ChIP experiments were performed in control or TRIM46-overexpressing MCF-7 cells with antibodies against HDAC1. HDAC1-associated DNAs were amplified using non-biased conditions, labeled, and then sequenced via HiSeq 2500. Using model-based analysis for ChIP-seq (MACS2) and a *P*-value cutoff of 10^{-3} , we identified 18,380 HDAC1 peaks in control MCF-7 cells and 15,347 HDAC1 peaks in TRIM46-overexpressing cells, observing a 16.5% reduction upon TRIM46 overexpression (Fig 5A).

We then performed transcriptome analysis in TRIM46-deficient cells using RNA deep sequencing (RNA-seq). In these experiments, total RNAs were extracted from control or TRIM46-depleted MCF-7 cells. Samples from biologically replicated experiments were then sequenced via BGISEQ-500. Genes that were differentially expressed in both experiments were considered to be subjected to TRIM46 regulation. Among 630 differentially expressed genes upon depletion of TRIM46, 292 were upregulated and 338 were downregulated (Fig 5B). Since TRIM46 promotes the degradation of HDAC1, a transcription corepressor, we reasoned that genes in the downregulated group are more likely to be the targets of the TRIM46-HDAC1 axis. RNA-seq results were then cross-analyzed with the ChIP-seq results, in which HDAC1 targets were defined by peaks within -5 kb to $+5$ kb of the gene. Genes that were downregulated upon TRIM46 depletion and targeted by HDAC1 were considered to be the targets of the TRIM46-HDAC1 axis (Fig 5C). These genes were then classified into different cellular signaling pathways using MAS software with a *P*-value cutoff of $< 10^{-2}$. We found a significant enrichment of TRIM46-HDAC1 target genes in DNA replication, DNA repair/Fanconi anemia, and cell cycle pathways (Fig 5C and D). We verified the results by qPCR analysis of the expression of selected genes, including PRIM2, MCM2, MCM5, POLA2, BLM, FANCI, FANCA, BRCA1, BRCA2, E2F1, and CDC45, which represent the classified pathways. We found that overexpression of TRIM46 in MCF-7 cells led to a significant increase in the expression of these genes, which was offset by co-overexpression of HDAC1 (Fig 5E). On the other hand, knockdown of TRIM46 in MCF-7 cells resulted in a significant decrease in the expression of these genes, which was effectively

reversed by co-knockdown of HDAC1 (Fig 5F). In addition, the decreased expression of these genes in TRIM46-depleted cells was successfully rescued by overexpression of siRNA-resistant full-length TRIM46 but not TRIM46 Δ RING (Fig 5G).

As HDAC1 and HDAC2 are closely related and often co-exist in the same transcriptional repression complexes, we further examined whether HDAC2 also regulated the TRIM46-HDAC1 target genes. ChIP qPCR experiments showed that HDAC2 was not recruited to most of the TRIM46-HDAC2 target promoters (Fig EV2B), and real-time qPCR showed that depletion of HDAC2 had the minimum effect of the gene expression, except for MCM5, POLA2, and BLM (Fig EV2C). However, overexpression of HDAC2 only partially abolished the effect of HDAC1 depletion (Fig EV2C), suggesting that HDAC1 plays a dominant role in regulating these genes. Together, these results support the regulation by the TRIM46-HDAC1 axis of genes involved in DNA replication/repair machinery in breast cancer cells.

The observation that the TRIM46-HDAC1 axis regulates DNA replication/repair factors such as DNA polymerases POLA2 and MCM2/MCM5 suggests that dysregulation of replication could be at least one of the mechanisms underlying SNP rs4971059-mediated breast carcinogenesis. We thus first performed FACS analysis to compare cell cycle profiles in control and TRIM46-depleted MCF-7 cells. In these experiments, MCF-7 cells were synchronized at the G₁/S boundary by a double-thymidine block. After release, TRIM46-depleted cells proceeded through cell cycle with an extended S phase and significantly slower pace, which could be rescued, at least partially, by co-knockdown of HDAC1 (Fig 6A), supporting a role for the TRIM46-HDAC1 axis in regulating DNA replication thus cell proliferation. We further performed EdU incorporation assays in TRIM46-deficient MCF-7 cells or TRIM46 and HDAC1 co-depleted MCF-7 cells. Knockdown of TRIM46 resulted in a significant decrease in the percentage of cells in the S phase, which was effectively rescued by simultaneously knockdown of HDAC1 (Fig 6B). We also performed experiments in normal mammary epithelial MCF-10A cells, in which the expression of TRIM46 was significantly lower than that in MCF-7 and other commonly used breast cancer cell lines (Fig 6C). Overexpression of TRIM46 in MCF-10A cells resulted in a significant increase in the percentage of cells in S phase, which was effectively rescued by simultaneously overexpression of HDAC1 (Fig 6B). Together, these observations indicate that

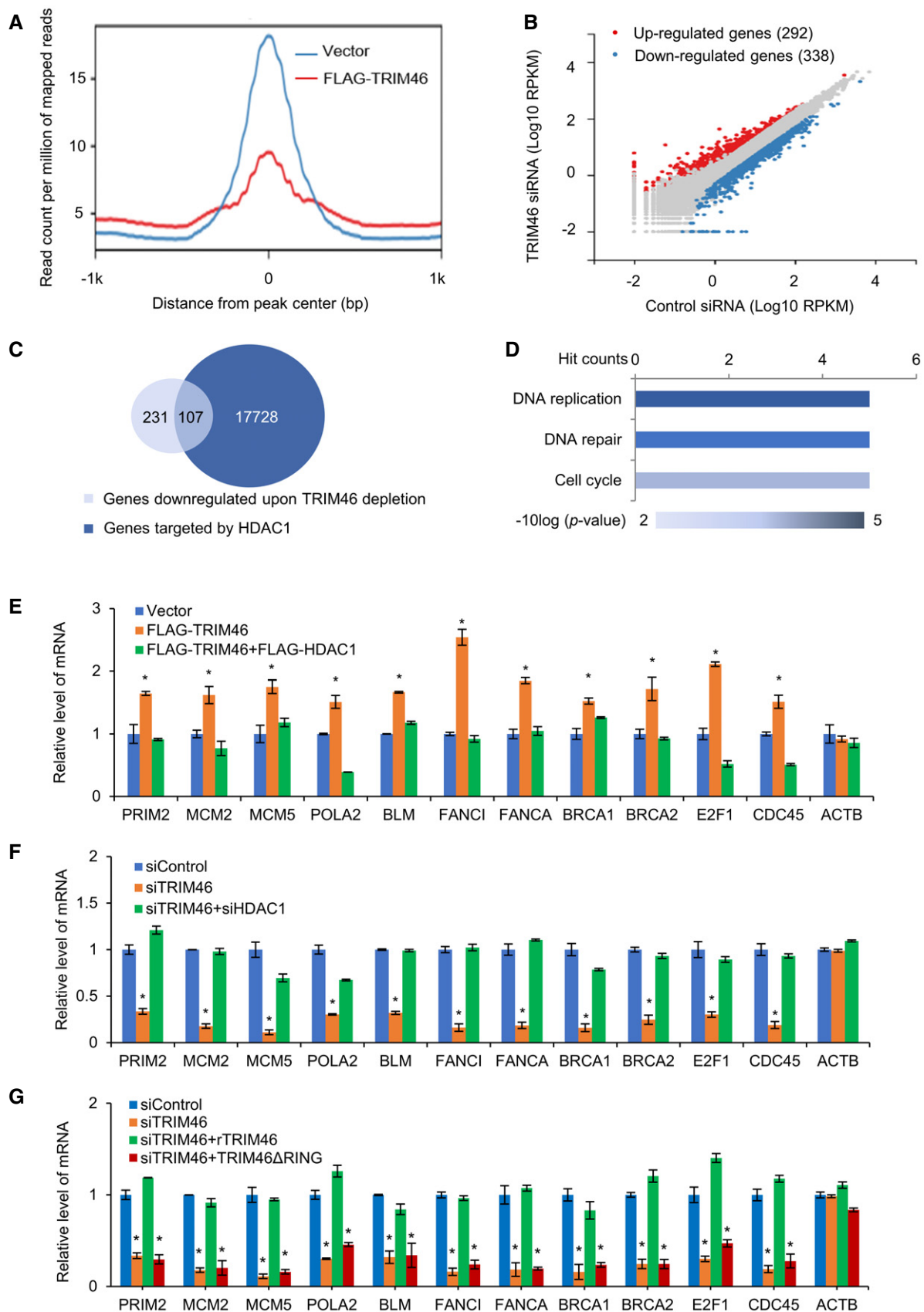


Figure 5.

Figure 5. The TRIM46-HDAC1 axis intersects with DNA replication and repair pathways.

- A ChIP-seq analysis was performed in control or TRIM46-overexpressing MCF-7 cells with antibodies against HDAC1. Density distributions (read count per million of mapped reads) of HDAC1 peaks were analyzed by deepTools.
- B Scatter plot of RNA-Seq data comparing genes between control and TRIM46-depleted MCF-7 cells. The clustering of the 630 differentially expressed genes is shown. RNA-seq experiments were performed in duplicate, and overlapping genes were analyzed.
- C The Venn diagram of overlapping target genes of the TRIM46-HDAC1 axis detected by ChIP-seq and RNA-seq.
- D Classification of genes targeted by the TRIM46-HDAC1 axis using Kyoto Encyclopedia of Genes and Genomes (KEGG) pathway analysis.
- E–G Verification of representative genes targeted by the TRIM46-HDAC1 axis. (E) MCF-7 cells were transfected with empty vector, FLAG-TRIM46, or FLAG-TRIM46 together with FLAG-HDAC1 for 48 h. (F) MCF-7 cells were transfected with control siRNA, TRIM46 siRNA, or TRIM46 siRNA together with HDAC1 siRNA for 72 h. (G) MCF-7 cells were transfected with control siRNA, TRIM46 siRNA, or a siRNA-resistant TRIM46 construct together with TRIM46 siRNA for 72 h. Total RNAs were extracted from cells, and RT-qPCR was performed with primers specific for indicated genes.

Data information: In (E–G), each bar represents the mean \pm SD for triplicate experiments (* P < 0.05, two-tailed unpaired t -test).

the TRIM46-HDAC1 axis influences DNA replication thus cell proliferation.

Among TRIM46-HDAC1 target genes, MCM2 and MCM5 are two components of the MCM complex, the replicative helicase essential for unwinding duplex DNA to promote fork progression (Liu *et al*, 2017). To gain further support of the role of the TRIM46-HDAC1 pathway in DNA replication, we next tested the effect of TRIM46-HDAC1 on MCM helicase activity. To this end, we treated MCF-7 cells with hydroxyurea (HU), which depletes nucleotide pool thus leads to the inhibition of DNA polymerase and the formation of single-stranded DNA (ssDNA). We found that upon HU treatment, the majority of S-phase MCF-7 cells generated ssDNA patches, which was largely impeded upon knockdown of TRIM46. However, the impaired ssDNA formation in TRIM46-depleted cells were successfully restored by co-knockdown of HDAC1 (Fig 6D). Moreover, DNA fiber assays (Burgers & Kunkel, 2017) in MCF-7 cells showed that knockdown of TRIM46 significantly hindered replication fork progression, whereas co-knockdown of HDAC1 could restore replication fork progression (Fig 6E). Collectively, the above data support that the TRIM46-HDAC1 axis promotes DNA replication, consistent with its role in the regulation of DNA replication factors such as MCM2, MCM5, POLA2, and CDC45.

The TRIM46-HDAC1 axis also regulates several key players involved in DNA damage responses, such as BLM, BRCA1, and

EXO1, which exert specific roles in the repair of double-strand breaks (Symington, 2016). To further explore the functional significance of the TRIM46-HDAC1 axis, we next tested the effect of TRIM46 on cell apoptosis and survival in response to the chemotherapeutic reagent cisplatin, which is known to cause double-strand DNA breaks in cells (Zhu *et al*, 2018). In these experiments, MCF-7 cells transfected with TRIM46 siRNA or co-transfected with TRIM46 siRNA and HDAC1 siRNA were treated with cisplatin. Flow cytometry analysis showed that depletion of TRIM46 in MCF-7 cells resulted in a significant increase in the percentage of apoptotic cells when exposed to cisplatin, an effect that could be effectively offset by co-depletion of HDAC1 (Fig 6F). Consistently, analysis by Western blotting revealed that treatment with cisplatin led to an overt increase in the level of γ H2AX in TRIM46-depleted cells, whereas depletion of HDAC1 in these cells restored cisplatin-induced γ H2AX (Fig 6G). These observations support a notion that the TRIM46-HDAC1 axis is implemented in DNA damage response in MCF-7 cells, at least for cisplatin insult.

TRIM46 promotes breast carcinogenesis and chemoresistance

Given the impact of the TRIM46-HDAC1 axis on DNA replication and damage response, we next investigated the potential role of this pathway in the carcinogenesis and chemotherapy of breast cancer.

Figure 6. The TRIM46-HDAC1 pathway functions in DNA replication and repair in breast cancer cells.

- A MCF-7 cells treated with control siRNA, TRIM46 siRNA, or TRIM46 siRNA and HDAC1 siRNA were synchronized by a double-thymidine block and released for 0 h, 12 h, 30 h, 36 h, or 42 h, respectively. Cell cycle progression after releasing was analyzed by flow cytometry.
- B Edu assays were performed in MCF-7 cells treated with control siRNA, TRIM46 siRNA or TRIM46 siRNA and HDAC1 siRNA for 72 h, or MCF-10A cells treated with vector, FLAG-TRIM46 or FLAG-TRIM46 and FLAG-HDAC1 for 48 h. Representative images from FACS analysis are shown on the left panel, the percentage numbers of cells in S phase were quantified by FlowJo software on the right panel.
- C Western blotting analysis of TRIM46 protein expression in different breast cell lines.
- D ssDNA formation in siRNA-treated MCF-7 cells after HU treatment. BrdU (20 μ g/ml) was added during the last 24 h of siRNA treatment and was removed by a brief wash prior to HU treatment (4 mM, 2 h), pre-extraction, and fixation. BrdU in ssDNA patches and PCNA were detected without a DNA denaturation step. Scale bar, 10 μ m. Diagrams show the frequency of PCNA-positive BrdU foci.
- E DNA fiber analysis of the rate of replication elongation. SiRNA-treated MCF-7 cells were sequentially pulse-labeled with 50 μ M IdU and 50 μ M CldU, each for 30 min. A sketch delineating experimental design and representative images of dual-labeled fibers are shown. Bars represent the median CldU tract length (n = 200 in each group). **** P < 0.0001, two-tailed unpaired t -test.
- F MCF-7 cells treated with control siRNA, TRIM46 siRNA or TRIM46 siRNA and HDAC1 siRNA were treated with 4 μ M cisplatin for 48 h and then double-stained with annexin V and propidium iodide. Cell apoptosis was determined by flow cytometry. Representative images from FACS analysis are shown on the left panel, the percentage of apoptotic cells was quantified by FlowJo software on the right panel.
- G Accumulation of γ H2AX in cells depleted of TRIM46 or HDAC1 after cisplatin stimulation. MCF-7 cells were treated with 4 μ M cisplatin for 8 h before harvesting. Cell lysates were analyzed by Western blotting.

Data information: In (B, D, and F), each bar represents the mean \pm SD for biological triplicate experiments (* P < 0.05, ** P < 0.01, two-tailed unpaired t -test).

Source data are available online for this figure.

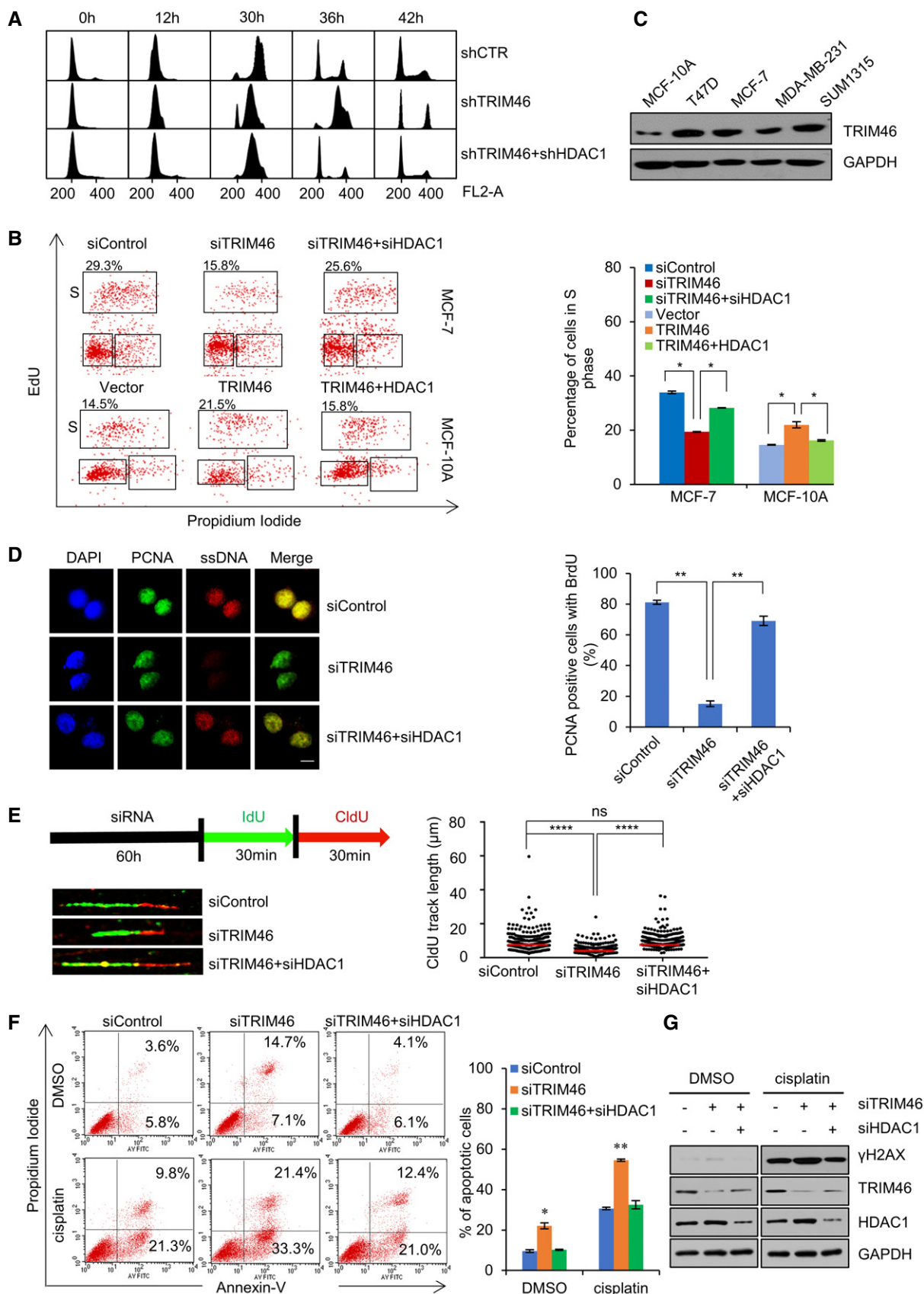


Figure 6.

Both MTS assays and colony formation assays revealed that depletion of TRIM46 had a significant inhibitory effect on breast cancer cell proliferation, which could be rescued by either overexpression of siRNA-resistant wild-type TRIM46, but not TRIM46 Δ RING, or co-knockdown of HDAC1. On the other hand, overexpression of TRIM46 was associated with an accelerated proliferation of both MCF-10A cells and MCF-7 cells, which was effectively neutralized by simultaneous overexpression of HDAC1 (Fig 7A and B).

To investigate the role of the TRIM46-HDAC1 axis in the growth of breast cancer *in vivo*, we infected MCF-7 cells with lentiviruses carrying control, TRIM46, or TRIM46 + HDAC1 or with lentiviruses carrying control shRNA, shTRIM46, or shTRIM46 + shHDAC1. These cells were then orthotopically implanted onto the abdominal mammary fat pad of 6-week-old female immunocompromised severe combined immunodeficiency (SCID) mice ($n = 6$). Tumor growth was monitored weekly for eight weeks. The results showed that overexpression of TRIM46 promoted the growth of the primary tumor, an effect that was counteracted by overexpression of HDAC1. Conversely, depletion of TRIM46 suppressed breast tumor growth, a phenotype that was offset by co-depletion of HDAC1 (Fig 7C).

We then treated TRIM46-deficient MCF-7 cells with several chemotherapeutic drugs for breast cancer, including cisplatin, adriamycin, and etoposide (VP16), and cell viability was examined by Alamar blue staining. The results showed that loss-of-function of TRIM46 was associated with a significant decrease in the number of viable MCF-7 cells upon treatment of all the three agents (Fig 7D). In addition, gain-of-function assays performed in MCF-10A cells indicated that overexpression of TRIM46 led to a significant increase in cell viability upon treatment with these agents (Fig 7E), supporting a role of TRIM46 in promoting chemoresistance. Together, the above results point an important role for the TRIM46-HDAC1 axis in the proliferation and chemoresistance of breast cancer cells.

High expression of TRIM46 is correlated with aggressive clinical behaviors of breast cancer

To support the role of the TRIM46-HDAC1 pathway in breast carcinogenesis and to extend our observations to a clinicopathologically relevant context, we next assessed, by immunohistochemical staining, the protein level of TRIM46 and HDAC1 in breast cancer using tissue arrays containing 142 breast carcinoma samples from patients with grade I (29), II (69), or III (44) breast cancer. Analysis using Image-Pro Plus software showed that TRIM46 expression is significantly upregulated and HDAC1 expression is markedly downregulated in breast carcinoma samples. In addition, statistical analysis showed that the level of TRIM46 expression is positively correlated with the histological grades of the tumors, whereas the level of HDAC1 expression is negatively correlated with grades of the tumors (Fig 8A). We further collected 20 samples of breast cancer paired with adjacent normal mammary tissues and analyzed by western blotting for the expression of TRIM46 and HDAC1. The results showed that overall TRIM46 expression is higher in tumor samples than in adjacent tissues, whereas HDAC1 expression exhibited a reverse trend (Fig 8B and C). Moreover, analysis of the public dataset (TCGA) revealed that the mRNA levels of TRIM46, BRCA1, and BLM are all upregulated in breast cancer (Fig 8D), and interrogation of Miyake's breast cancer dataset in Oncomine (<https://www.oncomine.org/>) as well as the public dataset GSE21653

showed that the levels of TRIM46, BRCA1, and BLM are all positively correlated with the histological grades of breast cancer (Fig EV3A). Furthermore, analysis of the public datasets GSE36774 and GSE21653 revealed that the mRNA level of TRIM46 is significantly positively correlated with that of BRCA1 and BLM, two target genes of the TRIM46-HDAC1 axis, in breast carcinomas (Fig EV3B). Finally, Kaplan–Meier survival analysis of the TCGA dataset showed that higher expression of either TRIM46, BRCA1, or BLM is associated with poor overall survival of breast cancer patients (Fig 8E). The results of the statistical tests for all breast cancer datasets are provided in Table EV4. We noticed that the correlative expression of TRIM46 with BRCA1 or with BLM was not validated in TCGA-Breast and Miyake's breast. The differential results may be due to several factors such as sample size, detection methods, tumor subtypes, and/or ethnic bias. Collectively, these observations are consistent with the role of the TRIM46-HDAC1 axis in breast carcinogenesis.

Discussion

In the current study, we linked SNP rs4971059A-associated breast cancer risk to dysregulated TRIM46 function. SNP rs4971059 is one of the 65 new breast cancer risk loci identified in recent genome-wide association analysis. We find that SNP rs4971059 locates at the 6th intron of *TRIM46* that functions as an active enhancer. G to A polymorphic switch of the rs4971059 allele augments its chromosomal interaction with the promoter and boosts its enhancer activity. Change of endogenous SNP sequence from G to A using CRISPR/Cas9-mediated homologous recombination leads to an overt upregulation of TRIM46. We then collected 90 breast tumor samples and found that the risk allele rs4971059A was strongly correlated with an increased expression of TRIM46. Interestingly, the frequency of SNP[A] rs4971059 is different in European and Asian populations. The frequency of SNP[A] rs4971059 in global population is 0.4299 or 0.3798 as recorded in 1000G or HapMap database. However, this frequency is as high as 0.7599 or 0.829 in East Asian people. In our hands, we detected 16 [GA] and 71 [AA] genotypes out of 90 samples from east Asian ethnic origin, representing 87.78% (158/180) of A allele frequency for breast cancer patients. As variants identified in GWAS studies often account for small percentages of the observed phenotype, which is ultimately determined by the sum of complex and counteracting genetic background, it is important to expand the sample origins and further study the TRIM46-mediated breast carcinogenesis in other populations. In addition, we found that the expression of TRIM46 is different for paired breast tumors and their adjacent normal tissues, whereas the genotypes are the same (Table EV3). Since the level of gene expression is eventually determined by both cis-regulatory elements and transcription factors/cofactors, we are currently investigating the upstream regulatory factors that may contribute to the altered expression of TRIM46 in breast cancer.

Besides TRIM46, we noticed that the expression of several other genes proximal to SNP rs4971059 was also changed upon the G to A switch by gene editing, such as increased MUC1 expression and decreased THBS3 and MIR92b expression (Fig 1F). MUC1 is a cell surface glycoprotein often overexpressed in multiple carcinomas, including breast cancer (Jing *et al*, 2019). THBS3 belongs to the

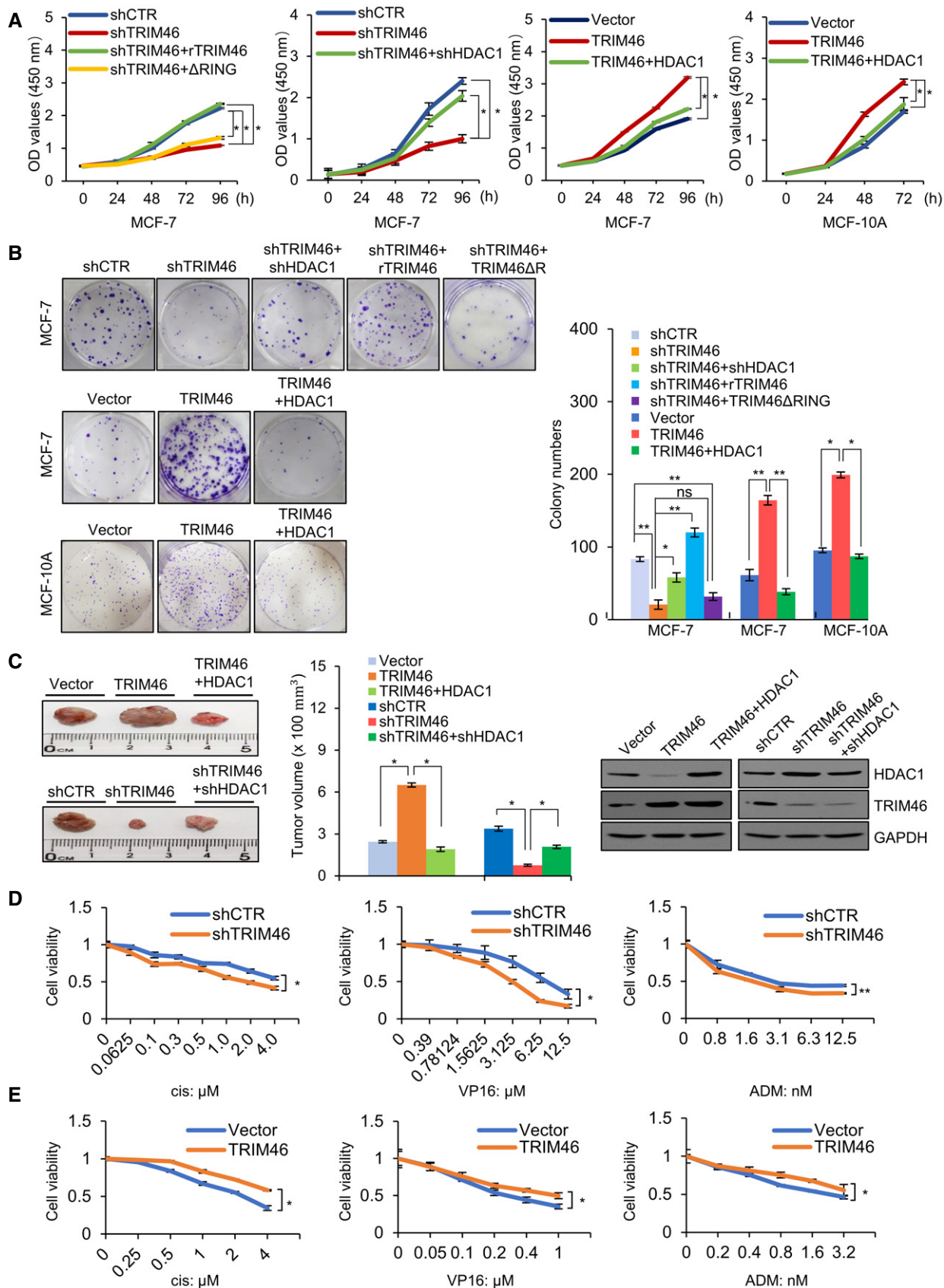


Figure 7.

Figure 7. TRIM46 promotes breast carcinogenesis and chemoresistance.

- A MCF-7 cells or MCF-10A cells were infected with lentiviruses carrying the indicated constructs. Cells were split into 96-well plates and then harvested at the indicated day. Cell growth curves were measured with MTS assays.
- B MCF-7 cells stably transfected with indicated shRNAs or expression plasmids or MCF-10A cells stably transfected with expression plasmids were tested for colony formation assay.
- C MCF-7 cells infected with lentiviruses carrying indicated plasmids were inoculated into the left abdominal mammary fat pad (5×10^6 cells) of 6-week-old immunocompromised female SCID beige mice. Tumor size was measured after 8 weeks (mammary tumors, $n = 6$). The efficiency of overexpression or knockdown of the gene was verified by Western blotting.
- D Control MCF-7 cells or MCF-7 cells depleted with TRIM46 were treated with different concentrations of cisplatin (cis), VP16, or adriamycin (ADM) for 72 h, and the proportions of viable cells were examined.
- E Control MCF-10A cells or MCF-10A cells overexpressed TRIM46 were treated with different concentrations of cisplatin, VP16, or adriamycin for 72 h, and the proportions of viable cells were examined.

Data information: In (A-B, and D-E), each bar represents the mean \pm SD for biological triplicate experiments (* $P < 0.05$, ** $P < 0.01$, two-tailed unpaired t -test). In (C), each bar represents the mean \pm SD ($n = 6$, * $P < 0.05$, two-tailed unpaired t -test). Source data are available online for this figure.

thrombospondin family, whose function in cancer development is not clear (Vos *et al*, 1992). MIR92b (microRNA 92b) has been shown to suppress breast cancer cell viability and invasion by targeting EZH2 (Liu *et al*, 2018). Whether these genes also contribute to SNP rs4971059A-associated breast cancer risk needs further investigation.

Among all the TRIM family members, the biological function of TRIM46 is less understood. Previous studies report the role of TRIM46 in the nervous system, where TRIM46 is involved in the polarization of neuronal cells in the axon initial segment (van Beuningen *et al*, 2015), mainly through cooperating with KAP3 under the MAPK2 signaling to organize microtubule fasciculation (Harterink *et al*, 2019; Ichinose *et al*, 2019). TRIM46 may also have a role in gout, as two SNPs located downstream of *TRIM46* were potentially linked to serum urate levels (Kottgen *et al*, 2013; Dong *et al*, 2017). Notably, a previous report indicated that low expression of Trim46 was associated with inhibition of the proliferation and migration of 4T07 mouse breast cancer cells (Zhang *et al*, 2016). This result is consistent with our study showing that TRIM46 promotes breast cancer proliferation in humans. As we have demonstrated that TRIM46 functions as an E3 ligase and targets HDAC1 for proteasome-mediated degradation in breast cancer cells, it will be interesting to investigate whether TRIM46-mediated HDAC1 degradation also plays a role in neuronal development and the pathogenesis of gout.

How HDAC1 is associated with breast carcinogenesis is debatable. Overexpression of HDAC1 has been linked to accelerated breast cancer cell proliferation (Kawai *et al*, 2003). However, this conclusion is mainly based on *in vitro* experiments where cells were treated with TSA, an HDAC inhibitor known to have HDAC-independent activity (Chen *et al*, 2005). In contrast, immunohistochemistry staining indicated that HDAC1 expression is significantly reduced in ductal carcinoma *in situ* (DCIS) and invasive ductal carcinoma (IDC) compared to normal breast epithelium (Suzuki *et al*, 2009), an observation consistent with our results that HDAC1 is degraded by TRIM46 during breast carcinogenesis. It becomes increasingly clear that the potential application of HDAC1 inhibitors in breast cancer treatment should be re-evaluated, although these agents have shown promising effects to treat certain types of leukemia and other solid tumors (Minucci & Pelicci, 2006). Further in-depth mechanistic studies are required to understand the specificity and efficacy of HDAC inhibitors to treat cancer under different circumstances.

The intersection between the TRIM46-HDAC1 axis and the DNA replication/repair machinery is significant. TRIM46-mediated HDAC1 degradation in breast cancer cells alleviates transcriptional repression of many genes involved in DNA replication and repair to endow tumor cells with growth advantage and chemoresistance, which could be a molecular basis of the oncogenic activity of TRIM46 underlying the risk characteristics of SNP rs4971059 [A] in breast cancer. Among the target genes regulated by TRIM46-mediated HDAC1 degradation, a particularly interesting one is BRCA1, which plays a central role in DNA damage repair. It was found that cancer-associated mutations of BRCA1 could result in defective DNA damage repair and increased sensitivity to platinum-based chemotherapy (Mylavarapu *et al*, 2018). Moreover, upregulation of BRCA1 has been found in tamoxifen-resistant breast cancer cells and is responsible for the resistance of chemotherapy (Zhu *et al*, 2018), supporting our results that TRIM46-mediated HDAC1 degradation lead to upregulation of BRCA1 and chemoresistance of breast cancer cells. Interestingly, while HDAC1 targets a broad range of genes at the chromatin level, genes regulated by the TRIM46-HDAC1 axis are limited and significantly enriched in the replication and repair pathway. Since HDAC1 is engaged in multiple transcriptional repressor complexes with different target specificity, a possible explanation for such disproportion is that TRIM46 degrades HDAC1 in responding to a specific cellular microenvironmental cue(s). Insights into upstream events and integrative analyses of genomic binding of different HDAC1-containing complexes should help to address this issue. Alternatively, unidentified substrates of TRIM46 E3 ligase could also play a role in TRIM46-mediated breast carcinogenesis.

While HDAC1 acts as a negative regulator of DNA replication and repair in our system, we are aware that the role of HDAC1 could be more complicated and multifaceted. By co-knockdown of HDAC1 and HDAC2 or using inhibitors targeting both proteins, researchers have shown that loss of HDAC1,2 lead to an increase in H4K16ac, which is involved in nascent chromatin decompaction, leading to a reduction of replication fork velocity and an increase in replication stress response (Bhaskara *et al*, 2013; Bhaskara, 2015). In another study, HDAC1 and HDAC2 suppressed the expression of PR130, a regulatory subunit of the trimeric PP2A, leading to sustained phosphorylation of checkpoint kinases ATM and CHK1/CHK2 and early arrest in S phase (Goder *et al*, 2018). Both HDAC1 and HDAC2 could also be rapidly recruited to the DNA damage site to remove acetylation of H3K56, thereby promoting DNA nonhomologous end-

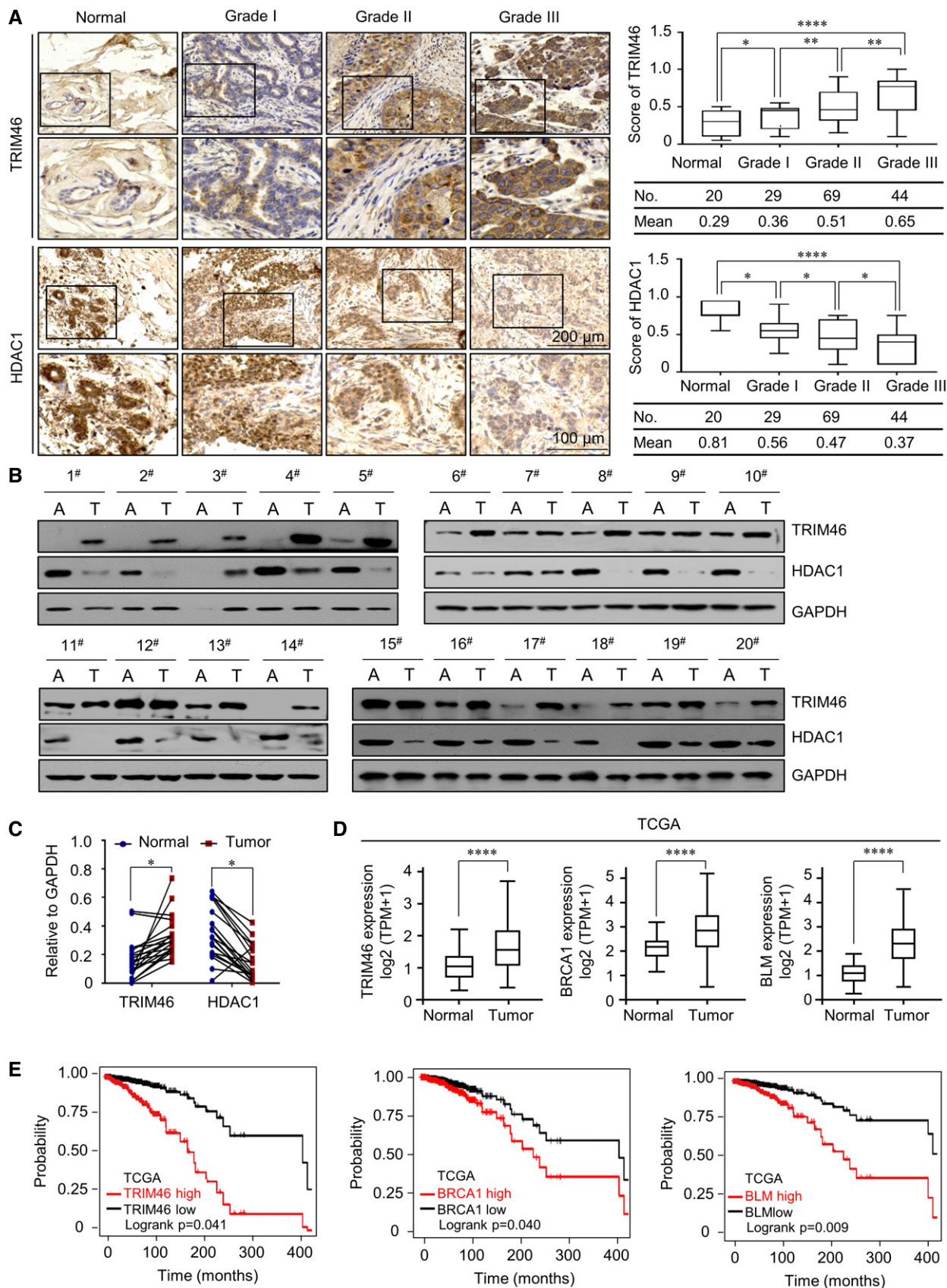


Figure 8.

Figure 8. The clinicopathological significance of the TRIM46-HDAC1 axis in breast cancer.

- A Immunohistochemical staining of tissue arrays containing 142 breast carcinoma samples (grade I: $n = 29$, grade II: $n = 69$, grade III: $n = 44$) and 20 normal mammary tissues for TRIM46 and HDAC1 expression. Representative images are shown on the left panel. The positively stained cells were analyzed, and the mean intensity was scored by Image-Pro Plus software on the right panel. In the boxplot, the central lines, the box limits, and the whiskers represented medians, 25th/75th percentile, and min/max, respectively. (* $P < 0.05$, ** $P < 0.01$, **** $P < 0.0001$, one-way ANOVA).
- B Total proteins from 20 paired samples of breast cancer "T" versus adjacent normal breast tissues "A" were extracted for western blotting analysis with antibodies against TRIM46 or HDAC1.
- C Quantification of the results in B by normalizing the protein level of TRIM46 or HDAC1 to that of GAPDH in "T" and "A" groups ($n = 20$). * $P < 0.05$, paired two-tailed Student's t -test.
- D Bioinformatics analysis of the public dataset from TCGA in breast carcinoma samples ($n = 1093$) and normal mammary tissues ($n = 112$) for the expression of TRIM46, BRCA1, or BLM based on the indicated stratifications (**** $P < 0.0001$, two-tailed unpaired t -test). In the boxplot, the central lines, the box limits, and the whiskers represented medians, 25th/75th percentile, and min/max, respectively.
- E Kaplan-Meier survival analysis of TCGA BRCA dataset for the correlation between overall survival of breast cancer patients and TRIM46, BRCA1, or BLM expression.

Source data are available online for this figure.

joining. However, these studies were also based on co-knockdown methods or inhibitors targeting all class I HDACs (Miller *et al*, 2010). As we demonstrated that most TRIM46-HDAC1 target genes were not regulated by HDAC2 (Fig EV2B and C), further mechanistic studies and more specific HDAC inhibitors will clarify how HDAC1 and HDAC2 play differential functions in replication and repair.

Materials and Methods

Antibodies and reagents

Commercial antibodies used for immunoblotting, immunoprecipitation, ChIP, immunofluorescence and immunohistochemical staining are collectively listed in Appendix Table S1. Anti-FLAG M2 affinity gel (A2220), FLAG peptide (F3290), MG132 (M9688), cycloheximide (AV31974), and doxycycline (D9891) were from Sigma. Protein A/G Dynabeads (10008D/10009D) were from Invitrogen. Ni-NTA agarose beads (30210) were from QIAGEN. Protease inhibitor mixture cocktail (4693116001) was from Roche Applied Science. Ubiquitinylation kit (BML-UW9920-0001) was from ENZO.

Plasmids and siRNAs

The cDNA of TRIM46 was cloned from HEK-293T cells. Deletion mutants of TRIM46 including TRIM46- Δ N, TRIM46- Δ C, and TRIM46- Δ RING were generated by subcloning corresponding fragments from TRIM46 cDNA. Deletion mutants of HDAC1 (HDAC1 Δ 1- Δ 4) were generated by subcloning corresponding fragments from FLAG-HDAC1 (Yang *et al*, 2011). HDAC1 mutants including HDAC1-K123R, HDAC1-K126R, HDAC1-K143R, and HDAC1-K144R were generated using QuikChange II Site-Directed Mutagenesis Kit. His-ubiquitin and HA-ubiquitin were described in the published paper (Han *et al*, 2014). The sequences of siRNA were as follows: control siRNA, 5'-UUCUCCGAACGUGUCACGU-3'; TRIM46 siRNA, 5'-GCUGACAAAGAGCCUGACA-3'; HDAC1 siRNA, 5'-CAACUAUGGUCUCUACCGA-3'. siRNAs were synthesized in GenePharma Inc (Shanghai, China).

Cell lines, cell culture, and transfection

The cell lines used were obtained from the American Type Culture Collection (ATCC). MCF-7 and HEK293T cells were maintained in

Dulbecco's modified Eagle's medium (DMEM) supplemented with 10% fetal bovine serum (FBS). MCF-10A cells were cultured in DMEM/F-12(1:1) medium supplemented with 5% horse serum, 20 ng/ml EGF, 500 ng/ml hydrocortisone, 100 ng/ml cholera toxin, and 10 μ g/ml insulin. Cells were maintained in a humidified incubator equilibrated with 5% CO₂ at 37°C. T-47D cells were cultured in RPMI-1640 medium supplemented with 10% FBS. MDA-MB-231 cells were cultured in L-15 medium supplemented with 10% FBS and without CO₂. SUM1315 cells were cultured in F-12 medium supplemented with 5% FBS, 5 μ g/ml insulin, 1 μ g/ml hydrocortisone, and 10 mM HEPES. Transfections of the siRNA oligonucleotides were carried out using RNAiMAX (Invitrogen) with the final concentration at 20 nM. Transfections of expression plasmids in MCF-7 cells were carried out using Neofect DNA transfection reagent (Neofect) according to the manufacturer's recommendations. Transfections of expression plasmids into MCF-10A cells were performed by electroporation (BTX ECM 830) with 8 pulses of 1200V according to the manufacturer's recommendations.

Genetic editing of SNP rs4971059 in MCF-10A cells using CRISPR/Cas9-mediated homologous recombination

The human codon-optimized SpCas9 px330 (Plasmid #42230) was obtained from Addgene (Mali *et al*, 2013). sgRNAs were designed and constructed as described previously (Mali *et al*, 2013; Hu *et al*, 2014). The DNA sequence of the region surrounding SNP rs4971059 was retrieved from the UCSC Genome Browser (Kent *et al*, 2002). Software tools predicting unique target sites are available online (<https://www.benchling.com/>). The Cas9 expression constructs were generated using the protocol as described (Ran *et al*, 2013). The sequences of donor DNAs were 500 bp upstream and downstream surrounding SNP rs4971059, with the site at SNP rs4971059 and PAM mutating. The sequence of sgRNA was 5'-GGTGGGGGTGCCTGGCATTG-3', and the sequences of donor DNAs were provided in Appendix Fig S1. The sgRNA and donor DNA were co-transfected into MCF-10A cells. After 3 days, 1.5 μ g/ml puromycin was added for at least three days for selection. Cells were subsequently sorted into 15 cm dishes with a density of \sim 5,000 cells/dish. Single cell-derived colonies were allowed to grow in dishes for 15 days. About two hundred clones were picked and screened for correct homologous recombination by PCR using specific primers that recognized SNP rs4971059 surrounding

sequences (Forward: 5'-CCTTCTGCAATGAGTGCTTCAA-3', Reverse: 5'-TCCTTTTGGAAACCCACAATG-3').

Immunopurification and mass spectrometry

MCF-7 cells stably expressing FLAG-TRIM46 were washed twice with cold PBS, scraped, and collected by centrifugation at 1,500 g for 5 min. Cells were lysed in lysis buffer (50 mM Tris-HCl pH 7.5, 150 mM NaCl, 0.3% NP-40, 2 mM EDTA) containing protease inhibitor cocktail for 40 min at 4°C. Anti-FLAG immunoaffinity columns were prepared using anti-FLAG M2 affinity gel following the manufacturer's suggestions. Cell lysates from 5×10^8 cells were applied to an equilibrated FLAG column of 1-ml bed volume. The mixture was incubated at 4°C for 3 h. After binding, the column was washed with cold PBS plus 0.1% Nonidet P-40. As described by the vendor, FLAG peptide was applied to the column to elute the FLAG protein complex. Fractions of the bed volume were collected and resolved on NuPAGE 4-12% Bis-Tris gel (Invitrogen), silver-stained using Pierce silver stain kit, and subjected to LC-MS/MS (Agilent 6340) sequencing.

Co-immunoprecipitation and western blotting

Cellular lysates were prepared by incubating MCF-7 cells in lysis buffer (50 mM Tris-HCl pH 7.5, 150 mM NaCl, 0.3% NP-40, 2 mM EDTA) containing protease inhibitor cocktail for 40 min at 4°C, followed by centrifugation at 14,000 g for 15 min at 4°C. The protein concentration of the lysates was determined using the BCA protein assay kit (Pierce) according to the manufacturer's protocol. Overall, 5% (1:20) cellular extracts were used for input. For immunoprecipitation, 500 µg of protein was incubated with 2 µg specific antibodies overnight at 4°C with constant rotation. 60 µl of 50% protein A or G agarose beads were then added, and the incubation was continued for an additional 3 h at 4°C. Beads were then washed five times using the wash buffer (50 mM Tris-HCl pH 7.5, 150 mM NaCl, 0.3% NP-40, 2 mM EDTA). Between washes, the beads were collected by centrifugation at 500 g for 5 min at 4°C. The precipitated proteins were eluted from the beads by resuspending the beads in 2× SDS-PAGE loading buffer and boiling for 10 min. The resultant materials from immunoprecipitation or cell lysates were resolved using 10% SDS-PAGE gel and transferred onto nitrocellulose membranes. For western blotting, membranes were incubated with appropriate antibodies for 1 h at room temperature or overnight at 4°C followed by incubation with a secondary antibody. Immunoreactive bands were visualized using Western blotting luminol reagent (Santa Cruz) according to the manufacturer's recommendation.

Luciferase reporter assays

We cloned a 3,251-bp fragment (Chr1: 155,171,860–155,174,110) containing TRIM46 promoter from total genomic DNA extracted from MCF-7 cells into a PGL3-basic vector to generate the PGL3-TRIM46 luciferase reporter (forward primer: 5'-AAGAGAAAAGATTAAGGGCAACC-3', reverse primer: 5'-TGTTCCAGGTCCCAGCTTG-3'). The 1.1-kb DNA sequence containing the [G] allele in the selected region in 1q22 were chemically synthesized and inserted into PUC57 vector. The sequence containing the [A] allele was generated using QuikChange II Site-

Directed Mutagenesis Kit. The 1.1-kb DNA sequence containing the [G] allele or [A] allele was then cloned into the PGL3-SV40 promoter or the PGL3-TRIM46 promoter. The constructs were confirmed by DNA sequencing. Co-transfection was performed with empty vector or the enhancer constructs and a Renilla luciferase reporter plasmid in MCF-7 cells. Cells were harvested after 24 h, and lysates were prepared for luciferase assays. At least three independent experiments were performed.

Annotation of SNP using HaploReg

HaploReg is a tool for exploring annotations of the noncoding genome at variants on haplotype blocks, such as candidate regulatory SNPs at disease-associated loci. HaploReg v4.1 (<http://pubs.broadinstitute.org/mammals/haploreg/haploreg.php>) was used to predict the potential functions of SNP rs4971059. The yellow box means "Weak Enhancer 2" (H3K4me1 and DNase enrichment), which is one of 25 chromatin states based on previous studies (Ernst & Kellis, 2015); orange box means "H3K4me1 Enhancer", and the black box means "missing data".

Chromosome conformation capture assays (3C)

The 3C assay was done essentially as described (Hagege *et al*, 2007) with minor modifications. Briefly, pellet from 1×10^7 MCF-7 cells was washed with PBS buffer and then crosslinked with formaldehyde (Sigma) in a final concentration of 2%. After a 10-min incubation at 37°C, glycine (0.125 M final concentration) was added to stop the reaction. The pellet was then subjected to cold lysis buffer with protease inhibitors, homogenized with a Dounce homogenizer on ice, and centrifuged to pellet the nuclei. To remove non-crosslinked proteins from DNA, SDS (Sigma) was added to a final concentration of 0.3%. For DpnII digestion, Triton X-100 (Sigma) was added to a final concentration of 1% to sequester excess SDS. A 5-µl aliquot of the sample was kept as an undigested genomic DNA control. DpnII (New England Biolabs) restriction enzyme was added to the remaining sample for overnight digestion at 37°C. Digestion efficiency was optimized and monitored by PCR using primer pairs designed specifically for each of the DpnII restriction sites in the locus. After complete digestion, 1.6% SDS was added for 20 min at 65°C to inactivate DpnII, and a 5-µl aliquot of the sample was set aside as the digested genomic DNA control. The ligation reaction was performed with 400 units of T4 DNA ligase (New England Biolabs) for 4 h at 16°C, followed by incubation for 30 min at room temperature in a total of 5-ml reaction system. Cross-linking was reversed by overnight incubation of the samples with proteinase K at 65°C, followed by phenol-chloroform purification of DNA. Purified DNA was subjected to PCR amplification with site-specific primer pairs. The primer and probe sequences are provided in Appendix Table S2.

GST pull-down assays

GST fusion constructs were expressed in BL21 *E. coli* bacteria, and crude bacterial lysates were prepared by sonication in TEDGN (50 mM Tris-HCl pH 7.4, 1.5 mM EDTA, 1 mM dithiothreitol, 10% (v/v) glycerol, 0.4 M NaCl) in the presence of the protease inhibitor mixture. In vitro transcription and translation experiments were done with rabbit reticulocyte lysate (TNT systems, Promega)

according to the manufacturer's recommendation. Briefly, equal amounts of GST fusion proteins were immobilized on 50 μ l of 50% glutathione-sepharose 4B slurry beads (Amersham Biosciences) in 0.5 ml of GST pull-down binding buffer (75 mM NaCl, 50 mM HEPES, pH 7.9). After incubation for 1 h at 4°C with rotation, beads were washed three times with GST pull-down binding buffer and resuspended in 0.5 ml of GST pull-down binding buffer before adding 10 μ l of *in vitro* transcribed/translated proteins for 2 h at 4°C with rotation. The beads were then washed three times with binding buffer. Bound proteins were eluted by boiling in 30 μ l of 2 \times sample loading buffer and resolved on SDS-PAGE.

Real-time RT-PCR

Total cellular RNAs were isolated from samples with TRIzol reagent (Invitrogen). First strand cDNA synthesis was performed with the Reverse Transcription System (TransGen Biotech). Quantitation of all gene transcripts was done by qPCR using Power SYBR Green PCR Master Mix and an ABI PRISM 7500 sequence detection system (Applied Biosystems) with the expression of GAPDH as the internal control. The sequences of primer pairs are provided in Appendix Table S3.

Ubiquitination assays

In vivo ubiquitination assays with immunoprecipitation was performed as previously described (Xirodimas *et al*, 2001; Lunyak *et al*, 2002). Briefly, cells were treated with MG132 before lysed in 2% SDS buffer containing 10 mM Tris-HCl pH 8.0, 150 mM NaCl and protease inhibitor. Lysates were boiled for 10 min followed by sonication for 2 min. Lysates were then diluted 1:10 in dilution buffer, incubated at 4°C for 30–60 min with rotation and centrifuged at 20,000 g for 30 min. Cellular extracts (0.5–1.5 mg) were incubated with anti-FLAG M2 affinity gel overnight. The beads were washed twice with washing buffer, boiled in SDS sample buffer and subjected to SDS-PAGE analysis. For *in vitro* ubiquitination assays, the reaction was carried out in 30 μ l ubiquitination buffer (50 mM Tris-HCl pH 7.5, 0.5 mM dithiothreitol) containing 200 nM E1 activating enzyme, 500 nM E2 conjugase, 15 μ g ubiquitin, 1 mM MgCl₂-ATP (all from Boston Biochem), 1 μ g TRIM46 WT/mutants, and 1 μ g HDAC1 that was incubated for 90 min at 30°C. The reaction was then directly subjected to Western blotting. For auto-ubiquitination assays, 2 μ g TRIM46 was incubated with E1, E2, and ubiquitin in reaction buffer for 90 min at 30°C, and the reaction was subjected to Western blotting analysis. The E2 conjugase kit provides a set of 10 commonly used E2 ubiquitin conjugating enzymes, including UBE2H, UBE2R1, UBE2D1, UBE2D2, UBE2D3, UBE2E1, UBE2E3, UBE2L3, UBE2C and UBE2N/UBE2V1.

ChIP sequencing

MCF-7 cells stably expressing vector and FLAG-TRIM46 were maintained in DMEM supplemented with 10% fetal bovine serum. Approximately 5 \times 10⁷ cells were used for each ChIP-seq assay. The chromatin DNA was precipitated by either normal rabbit IgG (control) or polyclonal antibodies against HDAC1. The DNA was purified with Qiagen PCR purification kit. In-depth whole genome DNA sequencing was performed by CapitalBio Corporation, Beijing. The

raw sequencing image data were examined by the Illumina analysis pipeline, aligned to the unmasked human reference genome (UCSC GRCh37, hg19) using Bowtie2, and further analyzed by MACS (Model-based Analysis for ChIP-Seq). Enriched binding peaks were generated after filtering through the control IgG. Genomic distribution of HDAC1, binding sites was analyzed by ChIPseeker, an R package for ChIP peak annotation, comparison and visualization (Yu *et al*, 2015). Pathway analysis was conducted based on the Database for Annotation, Visualization and Integrated Discovery (DAVID, <https://david.ncifcrf.gov/>; Huang *et al*, 2009). The profile plot for scores over sets of genomic regions was analyzed by deeptools, a suite of python tools for the sufficient analysis of high-throughput sequencing data.

RNA sequencing

MCF-7 cells were treated with control siRNA or siRNA of TRIM46 for 72 h. Total RNA was isolated and used for RNA-seq analysis. cDNA library construction and sequencing were performed by Beijing Genomics Institute using BGISEQ-500 platform. High-quality reads were aligned to the human reference genome (GRCh38) using Bowtie2. The expression levels for each of the genes were normalized to fragments per kilobase of exon model per million mapped reads (FPKM) using RNA-seq by Expectation Maximization (RSEM).

ChIP and qChIP

ChIP and qChIP were performed essentially the same as previously described (Si *et al*, 2015). DNA was purified with the QIAquick PCR Purification Kit. qChIPs were performed using the TransStart Top Green qPCR supermix (Trans-Gen Biotech). The primers are provided in Appendix Table S4.

Cell cycle synchronization and flow cytometry analysis

MCF-7 cells were synchronized in the G1/S phase by a double-thymidine block and were released for various hours (Cos *et al*, 1996). In all cases, cells were trypsinized, washed with PBS, and fixed in 70% cold ethanol at 4°C overnight. Cells were again washed with PBS and treated with 0.1 mg/ml RNase A (Sigma) for 30 min at 37°C and subsequently stained with 50 mg/ml propidium iodide (PI). Cell cycle data were collected using a FACS calibur flow cytometer (BD Biosciences) and analyzed with FlowJo 10. For EdU incorporation assays, MCF-7 cells were incubated with EdU in a final concentration of 10 μ M for 10 min. Then, cells were collected and analyzed according to the instructions of EdU Flow Cytometry Assay Kit (Life Technologies, C10419).

Detection of ssDNA

Detection of ssDNA was performed in MCF-7 cells as previously described (Groth *et al*, 2007). Briefly, cells were grown on six-well chamber slides, and BrdU (20 μ M) was added during the last 24 h of siRNA (specific for TRIM46 or HDAC1) treatment and removed by a brief wash prior to HU treatment (4 mM, 2 h). Cells were extracted 5 min with 0.5% cytoskeleton (CSK) buffer (10 mM PIPES pH 7, 100 mM NaCl, 300 mM sucrose, 3 mM MgCl₂) and rinsed with CSK and PBS before fixed 10 min in 100% methanol at room

temperature. Chamber slides were subsequently washed three times with PBS, treated with cold 70% ethanol at -20°C for 1 h, blocked with 1% BSA, and incubated with PCNA and BrdU antibodies followed by staining of FITC or TRITC-conjugated secondary antibodies. BrdU in ssDNA patches and PCNA were detected without a DNA denaturation step.

DNA fiber assays

DNA fiber assays to analyze replication fork progression and origin firing were essentially carried out as described previously (Kopper *et al.*, 2013). In brief, cells were pulse-labeled with 50 μM IdU (Sigma) for 30 min, followed by a second labeling with 50 μM CldU (Sigma) for 30 min before analysis. Cells were harvested and DNA fibers were stretched onto glass slides in a DNA lysis buffer (200 mM Tris-HCl pH 7.4, 0.5% SDS, 50 mM EDTA). After fixation with methanol/acetic acid (3:1), DNA was denatured with 2.5 M HCl and blocked (PBS with 1% BSA and 0.1% Triton X-100) before staining with mouse anti-IdU (BD), rat anti-CldU (Abcam), and the corresponding secondary antibodies conjugated with Alexa Fluor 488 or 555 (Invitrogen). Statistical analysis was performed using Prism 6 (GraphPad Software).

Apoptosis assays

MCF-7 cells were treated with 4 μM cisplatin or 0.1% DMSO as a control for 48 h. After harvest, cells were treated with Annexin V-FITC/PI Apoptosis Kit (Multisciences, China) and analyzed by flow cytometry (BD Accuri™ C6).

Cell viability/proliferation assays

For cell proliferation assays, MCF-7 or MCF-10A cells were seeded into 96-well plates with an equal volume of medium. On the day of harvest, the CellTiter 96® Aqueous ONE Solution Reagent (Promega) was added according to the manufacturer's protocol. Plates were incubated at 37°C for 1 h and cell viability was determined by measuring the absorbance of converted dye at wavelengths 490 nm. The detailed protocol is following the manufacturer's instruction (Promega). Each experiment was performed in triplicate and repeated at last three times.

Colony formation assays

MCF-7 or MCF-10A cells were maintained in culture media in 6-well plate for 14 days, fixed with 4% paraformaldehyde, stained with 0.1% crystal violet for colony observation, and counted using light microscope. Each experiment was performed in triplicate and repeated at last three times.

Mice and tumor xenografts

The SCID beige mice (6 weeks, female) were purchased from Peking University Health Science Center Department of Laboratory Animal Science. All animals were maintained in a standard pathogen-free facility. MCF-7 cells were infected with lentiviruses carrying the plasmids indicated in our study. 48 h after infection, 5×10^6 cells were injected into mammary fat pads of 6- to 8- week-old SCID

mice. Eight animals per group were used in each group. E2 pellets (0.72 mg per pellet, 60 d release; Innovative Research of America), or vehicle pellets were implanted 1 d before the tumor cell injection. All studies were approved by the Animal Care Committee of Peking University Health Science Center.

Patients and specimens

Tumor tissues were obtained from surgical specimens from patients with breast cancer. Samples were frozen in liquid nitrogen immediately after surgical removal and maintained at -80°C until protein extraction. Paired samples of breast cancer with adjacent normal mammary tissues and samples of breast cancers were obtained from the Breast Disease Center of Peking University People's Hospital and Peking University Third Hospital, and approved by the Ethics Committee of the Peking University Health Science Center.

Expression and eQTL analysis

The data of the genotype and gene expression were from the 90 breast cancers tissues. The clinical and pathologic characteristics of 90 cases are shown in Table EV1. The mean age of the patients was 68 years. Seventy cases were positive for estrogen receptor, sixty-eight cases were positive for progesterone receptor, and sixty-nine cases were positive for HER2. We perform the expression quantitative trait loci analysis using the R package "MatrixEQTL" version 2.3 (Shabalina, 2012). We used the function `Matrix_eQTL_main` with its default parameters (`pvOutputThreshold = 0.05`, `cisDist = 5e5`). Any variants with minor allele frequency of 0.05 were removed. The cis-eQTL was defined as variant-gene association within 500 bp of transcription start site (TSS). The P values and FDR were corrected for multiple testing using Bonferroni method.

Statistical analysis

Data from biological triplicate experiments are presented with error bar as mean \pm SD unless otherwise noted. Two-tailed unpaired Student's *t*-test was used for comparing two groups of data unless otherwise noted. Statistical significance was considered at a value of $P < 0.05$. SPSS version 13.0 was used for statistical analysis. Before statistical analysis, variation within each group of data, and the assumptions of the tests were checked. The correlation coefficients were calculated by R programming. The results of the statistical tests for all breast cancer datasets used in this study, such as TCGA BRCA dataset, GSE21653, GSE36774, and Miyake's breast dataset, were provided in Table EV4.

Data availability

ChIP-seq data for HDAC1 have been deposited in the Gene Expression Omnibus (GEO) with the accession number GSE176536 (<https://www.ncbi.nlm.nih.gov/geo/query/acc.cgi?acc=GSE176536>). RNA-seq data for TRIM46 have been deposited in the Gene Expression Omnibus (GEO) with the accession number GSE176537 (<https://www.ncbi.nlm.nih.gov/geo/query/acc.cgi?acc=GSE176537>). Breast data referenced in this study are available in GEO database (<http://www.ncbi.nlm.nih.gov/geo>) with the accession code numbers

GSE21653, GSE36774, and GSE32646 (Miyake's breast dataset). Data for Kaplan–Meier survival analysis in breast cancer patients are publicly available online at: <http://kmplot.com/analysis>.

Expanded View for this article is available online.

Acknowledgments

This work was supported by grant (2019YFA0508904 to J.L.) from the Ministry of Science and Technology of China, and grants (81730079 and 81530073 to Y.S., and 81861148027 and 81874161 to J.L.) from the National Natural Science Foundation of China.

Author contributions

YS and JLi conceived the project. JLi and ZZ designed the experiments. ZZ, JLi, and YS analyzed the data and wrote the manuscript. WL and LL provided bioinformatics support and advised on the SNP part. SW and JLi provided breast tumor samples and advised on the clinical correlation analysis. FP and JLi performed pathological analysis and provided technical support for IHC. ZZ, XL, YY, JY, YW, JW, XW, LSh, and LSu performed experiments and analyzed data.

Conflict of interest

The authors declare that they have no conflict of interest.

References

- Bhaskara S (2015) Histone deacetylases 1 and 2 regulate DNA replication and DNA repair: potential targets for genome stability-mechanism-based therapeutics for a subset of cancers. *Cell Cycle* 14: 1779–1785
- Bhaskara S, Jacques V, Rusche JR, Olson EN, Cairns BR, Chandrasekharan MB (2013) Histone deacetylases 1 and 2 maintain S-phase chromatin and DNA replication fork progression. *Epigenetics Chromatin* 6: 27
- Brunmeir R, Lagger S, Seiser C (2009) Histone deacetylase HDAC1/HDAC2-controlled embryonic development and cell differentiation. *Int J Dev Biol* 53: 275–289
- Burgers PMJ, Kunkel TA (2017) Eukaryotic DNA replication fork. *Annu Rev Biochem* 86: 417–438
- Calo E, Wysocka J (2013) Modification of enhancer chromatin: what, how, and why? *Mol Cell* 49: 825–837
- Chen CS, Weng SC, Tseng PH, Lin HP, Chen CS (2005) Histone acetylation-independent effect of histone deacetylase inhibitors on Akt through the reshuffling of protein phosphatase 1 complexes. *J Biol Chem* 280: 38879–38887
- Chen Y, Guo Y, Yang H, Shi G, Xu G, Shi J, Yin N, Chen D (2015) TRIM66 overexpression contributes to osteosarcoma carcinogenesis and indicates poor survival outcome. *Oncotarget* 6: 23708–23719
- Chen Y, Wang H, Yoon SO, Xu X, Hottiger MO, Svaren J, Nave KA, Kim HA, Olson EN, Lu QR (2011) HDAC-mediated deacetylation of NF- κ B is critical for Schwann cell myelination. *Nat Neurosci* 14: 437–441
- Choi JH, Kwon HJ, Yoon BI, Kim JH, Han SU, Joo HJ, Kim DY (2001) Expression profile of histone deacetylase 1 in gastric cancer tissues. *Jpn J Cancer Res* 92: 1300–1304
- Chu Y, Yang X (2011) SUMO E3 ligase activity of TRIM proteins. *Oncogene* 30: 1108–1116
- Cos S, Fernandez F, Sanchez-Barcelo EJ (1996) Melatonin inhibits DNA synthesis in MCF-7 human breast cancer cells in vitro. *Life Sci* 58: 2447–2453
- Dong Z, Zhou J, Jiang S, Li Y, Zhao D, Yang C, Ma Y, Wang YI, He H, Ji H et al (2017) Effects of multiple genetic loci on the pathogenesis from serum urate to gout. *Sci Rep* 7: 43614
- Eom M, Oh SS, Lkhagvadorj S, Han A, Park KH (2012) HDAC1 expression in invasive ductal carcinoma of the breast and its value as a good prognostic factor. *Korean J Pathol* 46: 311–317
- Ernst J, Kellis M (2015) Large-scale imputation of epigenomic datasets for systematic annotation of diverse human tissues. *Nat Biotechnol* 33: 364–376
- Göder A, Emmerich C, Nikolova T, Kiweler N, Schreiber M, Kühn T, Imhof D, Christmann M, Heinzel T, Schneider G et al (2018) HDAC1 and HDAC2 integrate checkpoint kinase phosphorylation and cell fate through the phosphatase-2A subunit PR130. *Nat Commun* 9: 764
- Gregoret IV, Lee YM, Goodson HV (2004) Molecular evolution of the histone deacetylase family: functional implications of phylogenetic analysis. *J Mol Biol* 338: 17–31
- Groth A, Rocha W, Verreault A, Almouzni G (2007) Chromatin challenges during DNA replication and repair. *Cell* 128: 721–733
- Hagege H, Klous P, Braem C, Splinter E, Dekker J, Cathala G, de Laat W, Forne T (2007) Quantitative analysis of chromosome conformation capture assays (3C-qPCR). *Nat Protoc* 2: 1722–1733
- Han X, Gui B, Xiong C, Zhao L, Liang J, Sun L, Yang X, Yu W, Si W, Yan R et al (2014) Destabilizing LSD1 by Jade-2 promotes neurogenesis: an antibraking system in neural development. *Mol Cell* 55: 482–494
- Harterink M, Vocking K, Pan X, Soriano Jerez EM, Slenders L, Fréal A, Tas RP, van de Wetering WJ, Timmer K, Motshagen J et al (2019) TRIM46 organizes microtubule fasciculation in the axon initial segment. *J Neurosci* 39: 4864–4873.
- Hassig CA, Fleischer TC, Billin AN, Schreiber SL, Ayer DE (1997) Histone deacetylase activity is required for full transcriptional repression by mSin3A. *Cell* 89: 341–347
- Hatakeyama S (2011) TRIM proteins and cancer. *Nat Rev Cancer* 11: 792–804
- Hatakeyama S (2017) TRIM family proteins: roles in autophagy, immunity, and carcinogenesis. *Trends Biochem Sci* 42: 297–311
- Herquel B, Ouararhni K, Khetchoumian K, Ignat M, Teletin M, Mark M, Bechade G, Van Dorsselaer A, Sanglier-Cianferani S, Hamiche A et al (2011) Transcription cofactors TRIM24, TRIM28, and TRIM33 associate to form regulatory complexes that suppress murine hepatocellular carcinoma. *Proc Natl Acad Sci USA* 108: 8212–8217
- Hu J, Lei Y, Wong W-K, Liu S, Lee K-C, He X, You W, Zhou R, Guo J-T, Chen X et al (2014) Direct activation of human and mouse Oct4 genes using engineered TALE and Cas9 transcription factors. *Nucleic Acids Res* 42: 4375–4390
- Huang da W, Sherman BT, Lempicki RA (2009) Systematic and integrative analysis of large gene lists using DAVID bioinformatics resources. *Nat Protoc* 4: 44–57
- Ichinose S, Ogawa T, Jiang X, Hirokawa N (2019) The spatiotemporal construction of the axon initial segment via KIF3/KAP3/TRIM46 transport under MARK2 signaling. *Cell Rep* 28: 2413–2426
- Jain AK, Allton K, Duncan AD, Barton MC (2014) TRIM24 Is a p53-Induced E3-ubiquitin ligase that undergoes ATM-mediated phosphorylation and autodegradation during DNA damage. *Mol Cell Biol* 34: 2695–2709
- Jing X, Liang H, Hao C, Yang X, Cui X (2019) Overexpression of MUC1 predicts poor prognosis in patients with breast cancer. *Oncol Rep* 41: 801–810
- Kawai H, Li H, Avraham S, Jiang S, Avraham HK (2003) Overexpression of histone deacetylase HDAC1 modulates breast cancer progression by negative regulation of estrogen receptor alpha. *Int J Cancer* 107: 353–358

- Kent WJ, Sugnet CW, Furey TS, Roskin KM, Pringle TH, Zahler AM, Haussler D (2002) The human genome browser at UCSC. *Genome Res* 12: 996–1006
- Kopper F, Bierwirth C, Schon M, Kunze M, Elvers I, Kranz D, Saini P, Menon MB, Walter D, Sorensen CS *et al* (2013) Damage-induced DNA replication stalling relies on MAPK-activated protein kinase 2 activity. *Proc Natl Acad Sci USA* 110: 16856–16861
- Köttgen A, Albrecht E, Teumer A, Vitart V, Krumsiek J, Hundertmark C, Pistis G, Ruggiero D, O'Seaghdha CM, Haller T *et al* (2013) Genome-wide association analyses identify 18 new loci associated with serum urate concentrations. *Nat Genet* 45: 145–154
- Lagger S, Meunier D, Mikula M, Brunmeir R, Schleder M, Artaker M, Puscho O, Egger G, Hagelkruys A, Mikulits W *et al* (2010) Crucial function of histone deacetylase 1 for differentiation of teratomas in mice and humans. *EMBO J* 29: 3992–4007
- Li YX, Seto E (2016) HDACs and HDAC inhibitors in cancer development and therapy. *Csh Perspect Med* 6: a026831
- Ling JQ, Li T, Hu JF, Vu TH, Chen HL, Qiu XW, Cherry AM, Hoffman AR (2006) CTCF mediates interchromosomal colocalization between Igf2/H19 and Wsb1/Nf1. *Science* 312: 269–272
- Liu F, Sang M, Meng L, Gu L, Liu S, Li J, Geng C (2018) miR92b promotes autophagy and suppresses viability and invasion in breast cancer by targeting EZH2. *Int J Oncol* 53: 1505–1515
- Liu Y, Liu S, Yuan S, Yu H, Zhang YU, Yang X, Xie G, Chen Z, Li W, Xu B *et al* (2017) Chromodomain protein CDYL is required for transmission/restoration of repressive histone marks. *J Mol Cell Biol* 9: 178–194
- Lunyak VV, Burgess R, Prefontaine GG, Nelson C, Sze SH, Chenoweth J, Schwartz P, Pevzner PA, Glass C, Mandel G *et al* (2002) Corepressor-dependent silencing of chromosomal regions encoding neuronal genes. *Science* 298: 1747–1752
- Mali P, Yang L, Esvelt KM, Aach J, Guell M, DiCarlo JE, Norville JE, Church GM (2013) RNA-guided human genome engineering via Cas9. *Science* 339: 823–826
- Micel LN, Tentler JJ, Smith PG, Eckhardt SG (2013) Role of ubiquitin ligases and the proteasome in oncogenesis: novel targets for anticancer therapies. *J Clin Oncol* 31: 1231–1238
- Michailidou K, Lindström S, Dennis J, Beesley J, Hui S, Kar S, Lemaçon A, Soucy P, Glubb D, Rostamianfar A *et al* (2017) Association analysis identifies 65 new breast cancer risk loci. *Nature* 551: 92–94
- Miller KM, Tjeertes JV, Coates J, Legube G, Polo SE, Britton S, Jackson SP (2010) Human HDAC1 and HDAC2 function in the DNA-damage response to promote DNA nonhomologous end-joining. *Nat Struct Mol Biol* 17: 1144–1151
- Minucci S, Pelicci PG (2006) Histone deacetylase inhibitors and the promise of epigenetic (and more) treatments for cancer. *Nat Rev Cancer* 6: 38–51
- Mylavarapu S, Das A, Roy M (2018) Role of BRCA mutations in the modulation of response to platinum therapy. *Front Oncol* 8: 16
- Ochs SD, Liu J, Fernando TM, Fecher RA, Sulentic CEW (2012) A dioxin response element in the multiple cloning site of the pGL3 luciferase reporter influences transcriptional activity. *Toxicol in Vitro* 26: 979–984
- Ran FA, Hsu PD, Wright J, Agarwala V, Scott DA, Zhang F (2013) Genome engineering using the CRISPR-Cas9 system. *Nat Protoc* 8: 2281–2308
- Santoro F, Botrugno OA, Dal Zuffo R, Pallavicini I, Matthews GM, Cluse L, Barozzi I, Senese S, Fornasari L, Moretti S *et al* (2013) A dual role for Hdac1: oncosuppressor in tumorigenesis, oncogene in tumor maintenance. *Blood* 121: 3459–3468
- Shabalin AA (2012) Matrix eQTL: ultra fast eQTL analysis via large matrix operations. *Bioinformatics* 28: 1353–1358
- Short KM, Cox TC (2006) Subclassification of the RBCC/TRIM superfamily reveals a novel motif necessary for microtubule binding. *J Biol Chem* 281: 8970–8980
- Si W, Huang W, Zheng YU, Yang Y, Liu X, Shan L, Zhou X, Wang Y, Su D, Gao J *et al* (2015) Dysfunction of the reciprocal feedback loop between GATA3- and ZEB2-nucleated repression programs contributes to breast cancer metastasis. *Cancer Cell* 27: 822–836
- Suzuki J, Chen YY, Scott GK, Devries S, Chin K, Benz CC, Waldman FM, Hwang ES (2009) Protein acetylation and histone deacetylase expression associated with malignant breast cancer progression. *Clin Cancer Res* 15: 3163–3171
- Symington LS (2016) Mechanism and regulation of DNA end resection in eukaryotes. *Crit Rev Biochem Mol Biol* 51: 195–212
- van Beuningen S, Will L, Harterink M, Chazeau A, van Battum E, Frias CP, Franker M, Katrukha E, Stucchi R, Vocking K *et al* (2015) TRIM46 controls neuronal polarity and axon specification by driving the formation of parallel microtubule arrays. *Neuron* 88: 1208–1226
- Venuto S, Merla G (2019) E3 ubiquitin ligase TRIM proteins, cell cycle and mitosis. *Cells* 8: 510
- Vogelstein B, Papadopoulos N, Velculescu VE, Zhou SB, Diaz LA, Kinzler KW (2013) Cancer genome landscapes. *Science* 339: 1546–1558
- Vos HL, Devarayalu S, de Vries Y, Bornstein P (1992) Thrombospondin 3 (Thbs3), a new member of the thrombospondin gene family. *J Biol Chem* 267: 12192–12196
- Wang J, Teng JL, Zhao D, Ge P, Li B, Woo PC, Liu CH (2016) The ubiquitin ligase TRIM27 functions as a host restriction factor antagonized by Mycobacterium tuberculosis PtpA during mycobacterial infection. *Sci Rep* 6: 34827
- Ward LD, Kellis M (2012) HaploReg: a resource for exploring chromatin states, conservation, and regulatory motif alterations within sets of genetically linked variants. *Nucleic Acids Res* 40: D930–D934
- Xirodimas D, Saville MK, Edling C, Lane DP, Lain S (2001) Different effects of p14ARF on the levels of ubiquitinated p53 and Mdm2 in vivo. *Oncogene* 20: 4972–4983
- Xue J, Chen Y, Wu Y, Wang Z, Zhou A, Zhang S, Lin K, Aldape K, Majumder S, Lu Z *et al* (2015) Tumour suppressor TRIM33 targets nuclear beta-catenin degradation. *Nat Commun* 6: 6156
- Yang X, Yu W, Shi L, Sun L, Liang J, Yi X, Li Q, Zhang YU, Yang F, Han X *et al* (2011) HAT4, a Golgi apparatus-anchored B-type histone acetyltransferase, acetylates free histone H4 and facilitates chromatin assembly. *Mol Cell* 44: 39–50
- You A, Tong JK, Grozinger CM, Schreiber SL (2001) CoREST is an integral component of the CoREST-human histone deacetylase complex. *Proc Natl Acad Sci USA* 98: 1454–1458
- Yu G, Wang LG, He QY (2015) ChIPseeker: an R/Bioconductor package for ChIP peak annotation, comparison and visualization. *Bioinformatics* 31: 2382–2383
- Zhang L, Li X, Dong W, Sun C, Guo D, Zhang L (2016) Mmu-miR-1894-3p inhibits cell proliferation and migration of breast cancer cells by targeting Trim46. *Int J Mol Sci* 17: 609
- Zhang Y, Ng HH, Erdjument-Bromage H, Tempst P, Bird A, Reinberg D (1999) Analysis of the NuRD subunits reveals a histone deacetylase core complex and a connection with DNA methylation. *Genes Dev* 13: 1924–1935
- Zhu Y, Liu Y, Zhang C, Chu J, Wu Y, Li Y, Liu J, Li Q, Li S, Shi Q *et al* (2018) Tamoxifen-resistant breast cancer cells are resistant to DNA-damaging chemotherapy because of upregulated BARD1 and BRCA1. *Nat Commun* 9: 1595